

895

SANDIA REPORT SAND82-2441 • Unlimited Release • UC-70
Printed April 1983

Empirically Determined Uncertainty in Potassium-Argon Ages For Plio-Pleistocene Basalts From Crater Flat, Nye County, Nevada

Scott Sinnock, Robert G. Easterling

Prepared by
Sandia National Laboratories
Albuquerque, New Mexico 87185 and Livermore, California 94550
for the United States Department of Energy
under Contract DE-AC04-76DP00789

8803300239 880308
PDR WASTE PDR
WM-11

Issued by Sandia National Laboratories, operated for the United States Department of Energy by Sandia Corporation.

NOTICE: This report was prepared as an account of work sponsored by an agency of the United States Government. Neither the United States Government nor any agency thereof, nor any of their employees, nor any of their contractors, subcontractors, or their employees, makes any warranty, express or implied, or assumes any legal liability or responsibility for the accuracy, completeness, or usefulness of any information, apparatus, product, or process disclosed, or represents that its use would not infringe privately owned rights. Reference herein to any specific commercial product, process, or service by trade name, trademark, manufacturer, or otherwise, does not necessarily constitute or imply its endorsement, recommendation, or favoring by the United States Government, any agency thereof or any of their contractors or subcontractors. The views and opinions expressed herein do not necessarily state or reflect those of the United States Government, any agency thereof or any of their contractors or subcontractors.

Printed in the United States of America
Available from
National Technical Information Service
U.S. Department of Commerce
5285 Port Royal Road
Springfield, VA 22161

NTIS price codes
Printed copy: A02
Microfiche copy: A01

Empirically Determined Uncertainty in Potassium-Argon Ages For Plio-Pleistocene Basalts From Crater Flat, Nye County, Nevada

Scott Sinnock
NNWSI Overview Division 9764

Robert G. Easterling
Statistics, Computing, and Human Factors Division 7223
Sandia National Laboratories
Albuquerque, NM 87185

Abstract

Six samples of basalt from each of four sites in Crater Flat, Nye County, Nevada, were dated by potassium-argon isotopic methods, by each of three separate geochronology laboratories. The mean ages of the four sites range from about 0.4 my (million years) to 4.0 my. The standard error of an age is 0.16 my, regardless of age. Variation among the reported ages can be attributed to aliquot, sample, and interlaboratory differences, with the latter two being dominant. The standard deviation of an age for a single sample dated by one laboratory is estimated as 0.34 my. Overall, the results indicate that Quaternary basalts with approximately 1.5% potassium content can be assigned an age at 90% confidence to within an interval of about 1 my if multiple samples are dated by several laboratories. If only one sample is dated by a single laboratory, the interval increases to about 1.4 my.

Acknowledgment

Sampling in 115°F heat in Crater Flat would have been less tolerable but for the assistance of Paul Damon and M. Shafiqullah (Shafi) from the University of Arizona; Bob Drake from the University of California Berkeley; Hal Krueger from Geochron; Bruce Crowe from Los Alamos National Laboratory; Will Carr from the United States Geological Survey (USGS); and Joe Fernandez of Sandia National Laboratories. Paul Damon, Shafiqullah, Bob Drake, Garniss Curtiss (Berkeley) and Hal Krueger performed the analytical work in support of this study. Field support was provided by Al Stephenson, Division 9764, and Adam Trujillo, Division 7135, of Sandia National Laboratories. The USGS graciously allowed use of its core library facility in Mercury, Nevada, for initial sample trimming and packaging during the June field expedition. Special appreciation is extended to Richard Marvin, USGS, and Bruce Crowe for their thoughtful reviews of a draft manuscript.

Contents

Introduction	7
Experiment Design	7
Results	8
Possible Sources of Uncertainty	13
Conclusions	13
Recommendations	14
Bibliography	15

Figures

1 Locations of Four Sampling Sites in Crater Flat, Nye County, Nevada	8
2 Histogram and Site Averages of Reported K-Ar Ages for Basalt Samples from Crater Flat, Nevada	10

Tables

1 Experiment Design for Investigating the Uncertainty in K-Ar Isotopic Ages	8
2 Reported K-Ar Ages, Precision Brackets, and Overall Site Means for Crater Flat Basalt Samples	9
3 Average Reported Ages, Standard Errors, Confidence Intervals, and Sources of Variance for Each Site in Crater Flat	11
4 Variance, Standard Deviation (σ), and Confidence Intervals for Potassium and Radiogenic Argon Measurements and Age Calculations for All 72 Samples	11
5 Reported Potassium and Argon Analyses of Crater Flat Basalts	12
6 Variance Estimates of Potassium and Argon Measurements for Subsamples and Samples	13

Empirically Determined Uncertainty in Potassium-Argon Ages For Plio-Pleistocene Basalts From Crater Flat, Nye County, Nevada

Introduction

This report presents results, conclusions, and recommendations from an experiment performed to assess uncertainty in potassium-argon (K-Ar) isotopic age determinations for late Cenozoic basalts. The purpose of this experiment is to statistically investigate the accuracy of K-Ar age determinations for relatively young basalts. Though many sources of variation affect such age determinations, it is often difficult to identify which ones are responsible for uncertainty in individual cases.

Users of isotopic dating methods commonly attempt to isolate causes of variation and compensate by rejecting anomalous samples, applying correction factors to calculated ages, and other means. However, a user of age dates who may not be associated with the isotopic laboratory commonly has no independent means by which to assess the confidence he can place in the accuracy of the reported ages. Isotopic laboratories as a matter of course report precision of calculated ages. Precision generally indicates only the reproducibility of a particular age given the sensitivity of laboratory instruments to conditions of a particular sample. This precision needs to be distinguished from the accuracy of the age determination, which depends on geological as well as laboratory sources of variation.

This experiment was designed to help an independent user estimate the accuracy of K-Ar age determinations for relatively young basalts. As such, the results and conclusions should be interpreted from the perspective of one who has sent a sample or set of samples to some independent isotopic laboratory for dating. When he receives a report on the ages determined by the laboratory, he may ask, "How accurate are the ages, and how do the true ages relate to the reported precision?" This experiment addresses these questions.

Because the purpose is to investigate confidence that a user can place in the age of a basalt sample

determined by any of a number of isotope laboratories and not to compare or evaluate individual laboratories, the data provided by each of the three participating laboratories are not identified by source in this report. To further preserve anonymity, perhaps at the expense of weakening the conclusions, distinctions among analytical techniques employed by the different laboratories are also not treated, except in a general sense, as a source of variation among the reported ages.

The experiment was supported by radioactive waste disposal investigations at the Nevada Test Site, Nye County, Nevada. These studies are conducted by the Department of Energy, through contracts with various laboratories and agencies, including Sandia National Laboratories (SNL).

Experiment Design

The experiment design consists of a matrix of six redundant K-Ar age determinations for each of four sampling sites by each of three laboratories: the Department of Geology and Geophysics, University of California, Berkeley campus; the Laboratory of Isotope Geochemistry, Department of Geosciences, University of Arizona, Tucson; and Geochron Laboratories Division, Krueger Enterprises Incorporated, Cambridge, Massachusetts (Table 1). The four sample sites are located in Crater Flat, Nye County, Nevada (Figure 1). At each site, four sample sets of basaltic rocks were collected in June 1979 by a group composed of geochronologists from each of the participating isotope laboratories and geologists from SNL, USGS, and Los Alamos National Laboratory. Each sample set was performed by physically breaking a single piece of basalt into separate pieces. Each laboratory received one piece from each set. Separate sample sets at each site were collected from separate

areas of the same outcrops, and all four sample sets from a single site were obtained within a general radius of about 20 to 30 m. The samples were cataloged, labeled, and sent to the three participating laboratories. Each laboratory was aware of the sampling location and known age constraints for each of the 16 samples so obtained.

Table 1. Experiment Design for Investigating the Uncertainty in K-Ar Isotopic Ages. Each set of six samples contained four identified and two unidentified samples.

	No. of Samples				Total
	Site 1	Site 2	Site 3	Site 4	
Berkeley	6	6	6	6	24
Arizona	6	6	6	6	24
Geochron	6	6	6	6	24
Total	18	18	18	18	72

each of the four sites. Eighteen samples were thus collected from each site, and each laboratory thus received 24 samples (Table 1).

Each isotope laboratory was provided orally with information regarding K-Ar age determinations by the USGS of basalt flows from the Crater Flat area. Lathrop Wells Cone. Site 1, had been dated previously as about 0.25 my. Red Cone. Site 2, is adjacent to and similar in terms of size and volume of flow material to Black Cone, previously dated as about 1.0 my.

Geomorphic characteristics show that Lathrop Wells Cone is essentially undissected, and the crater has not been breached by erosion. Black Cone is moderately dissected with small colluvial fans at the base of the cone. The remaining two sites, Sites 3 and 4, are dissected basalt outcrops protruding through the alluvial fill of east-central Crater Flat. Cone forms apparently have been removed by erosion, and only remnants of cone scoria remain in some places. Thus, geomorphic evidence indicates that Site 1, Lathrop Wells Cone, is the youngest; Site 2, Red Cone, is somewhat older (consistent with previous K-Ar age determinations); and Sites 3 and 4 are the oldest.

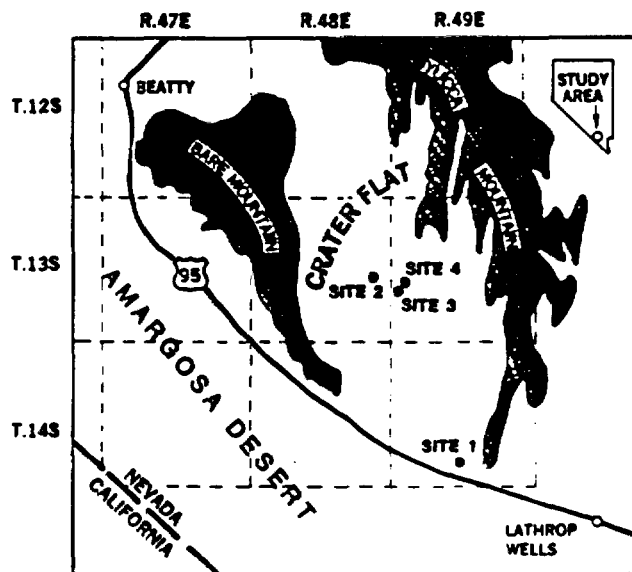


Figure 1. Location of Four Sampling Sites in Crater Flat, Nye County, Nevada

In August 1979, two additional sample sets were collected from each of the four sites without participation by the geochronologists. These were similarly subdivided, cataloged, and sent to the laboratories. However, samples from the second field expedition were labeled in a manner to prevent the geochronologists from knowing the sampling location or possible age constraints for individual samples. Thus, each laboratory received four identified samples and two unidentified samples for a total of six samples from

Results

Reported ages of the 72 samples and the average age for each site are given in Table 2 and Figure 2. The average of the individual precision brackets for each site reported by each laboratory also is included in Table 2. By inspection of the reported ages, it is clear that there are significant differences among the laboratories, as well as appreciable variation among samples from a given site. Laboratory A generally obtained older ages for most sites, and Laboratory B consistently obtained younger ages. For Site 1, Laboratory B reported two negative ages, an obviously impossible situation. This happened because the measured amount of radiogenic argon produced by potassium decay was less than that assumed to be present due to the atmospheric argon in the rock sample. Even for a single laboratory, it is apparent that variations among the reported ages for individual sites occur, though the standard deviation of the reported ages from a single laboratory agree quite well with the average of the reported precision. In some cases, e.g., Laboratories A and B, Site 1, the difference between identified and unidentified sample sites seems significant. When all reported ages from each site are considered, the standard deviation is generally much greater than reported precision. It is interesting to note that the standard deviations for each of the sites are about the same.

Table 2. Reported K-Ar Ages, Precision Brackets, and Overall Site Means for Crater Flat Basalt Samples

		Laboratory A		Laboratory B		Laboratory C	
S I T E 1	Mean Age Reported		0.73		0.08		0.57
	Standard Deviation		0.19		0.08		0.09
	Average Precision Reported		±0.11		±0.13		±0.12
	Sample Set	1	0.70 ± 0.07		0.12 ± 0.03		0.60 ± 0.09
		2	0.65 ± 0.07		-0.01 ± 0.29		0.61 ± 0.16
		3	0.77 ± 0.08		-0.03 ± 0.14		0.66 ± 0.10
	4	0.59 ± 0.06		0.08 ± 0.03		0.56 ± 0.09	
	5 ¹	1.1 ± 0.3		0.125 ± 0.18		0.59 ± 0.21	
	6 ¹	0.58 ± 0.08		0.175 ± 0.09		0.39 ± 0.07	
Mean Age Reported			1.53		1.12		1.55
Standard Deviation			0.31		0.27		0.15
Average Precision Reported			±0.19		±0.36		±0.20
S I T E 2	Sample Set	7	1.7 ± 0.2		0.965 ± 0.09		1.46 ± 0.11
		8	1.8 ± 0.2		0.95 ± 0.11		1.76 ± 0.19
		9	1.5 ± 0.2		0.975 ± 0.05		1.40 ± 0.13
		10	1.8 ± 0.2		1.66 ± 1.52		1.61 ± 0.24
		11 ¹	0.99 ± 0.15		1.08 ± 0.24		1.64 ± 0.35
		12 ¹	1.5 ± 0.2		1.11 ± 0.13		3.66 ± 0.14 ²
Mean Age Reported			4.27		3.73		3.89
Standard Deviation			0.46		0.06		0.17
Average Precision Reported			±0.45		±0.09		±0.32
S I T E 3	Sample Set	13	4.8 ± 0.5		3.637 ± 0.04		3.86 ± 0.11
		14	4.3 ± 0.5		3.815 ± 0.11		3.90 ± 0.92
		15	3.6 ± 0.4		3.78 ± 0.06		3.99 ± 0.12
		16	4.7 ± 0.5		3.745 ± 0.04		3.77 ± 0.32
		17 ¹	4.3 ± 0.3		3.695 ± 0.22		4.14 ± 0.13
		18 ¹	3.9 ± 0.5		3.73 ± 0.06		1.41 ± 0.38 ²
Mean Age Reported			4.22		3.69		4.00
Standard Deviation			0.08		0.09		0.13
Average Precision Reported			±0.32		±0.06		±0.12
S I T E 4	Sample Set	19	4.3 ± 0.3		3.79 ± 0.08		3.99 ± 0.10
		20	4.2 ± 0.3		3.795 ± 0.05		3.99 ± 0.12
		21	4.2 ± 0.3		3.555 ± 0.04		4.14 ± 0.11
		22	4.2 ± 0.3		3.64 ± 0.10		4.02 ± 0.12
		23 ¹	4.3 ± 0.3		3.68 ± 0.06		3.76 ± 0.11
		24 ¹	4.1 ± 0.4		3.705 ± 0.05		4.10 ± 0.15
				Overall Reported Ages from Each Site			
				<u>Mean Reported Age</u>		<u>Standard Deviation</u>	
Site 1 - Lathrop Wells Cone				0.46		0.31	
Site 2 - Red Cone				1.41		0.31	
Site 3 - Along Wash in Central Crater Flat				3.96		0.35	
Site 4 - Flow on Ridge Top in Central Crater Flat				3.97		0.24	

¹Unidentified samples

²Apparently labels of samples were interchanged, ages were switched between sample sets for the statistical analysis, including the calculation of means shown in this table. In the analysis all ages were rounded to two decimals.

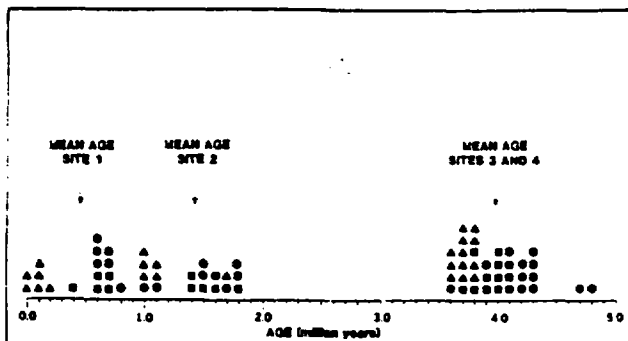


Figure 2. Histogram and Site Averages of Reported K-Ar Ages for Basalt Samples from Crater Flat, Nevada. Squares, circles and triangles represent ages of individual samples reported by different laboratories.

A statistical analysis of variance was performed to separate and identify sources of these apparent variations. Sources of variation considered were differences among sites, differences between sample collections, differences among samples, and differences among laboratories. The analysis of variance was done for each site separately and for the four sites combined. It shows that sample-to-sample and laboratory-to-laboratory variation dominate the total variation of the reported ages. Thus, the accuracy of a K-Ar age determination for the basalts of this experiment depends on both the number of laboratories and the number of samples analyzed by each laboratory.

Table 3 shows the average ages, standard errors,* computed confidence intervals, and sources of variance by category for specific sites and overall reported ages. Standard errors were calculated from the 18 reported ages for each site and did not consider the precision values reported by the laboratories. Estimated variances due to sampling and interlaboratory differences are similar for the four sites, suggesting that for basalts of this age range, the absolute uncertainty of K-Ar age determinations is constant, but relative dispersion is greater for younger rocks.

Confidence intervals for actual ages of the sites were calculated from the standard error of 0.16 my and indicate an uncertainty of about ± 0.5 my at 90% confidence and about ± 0.7 my at 95% confidence, independent of age. These uncertainty brackets pertain to age estimates obtained when 18 ages are reported by each of three laboratories for a single site. For a single sample dated by a randomly selected laboratory, the uncertainty is somewhat greater. In this case, the standard error is 0.34 my, and the 90% and 95% confidence intervals are about ± 0.7 or ± 0.9

*Standard error is a measure of how age estimates might vary if the experiment were repeated.

my, respectively (Table 4).^{*} Uncertainty in age estimates, when considering laboratory-to-laboratory variation is therefore somewhat greater than the precision reported by individual laboratories (Table 2).

The ages reported in Table 2 were calculated from measurements of potassium and radiogenic argon contained in the basalt samples. By inspection of Table 5, it is apparent that significant differences occur among the potassium and argon analyses of the individual laboratories.

Analysis of variance of the potassium and argon measurements (Table 4) shows differences among sample collections in that the two collections differ by more than the variation among individual samples can account for. This variability is attributed to "Experimental Factors" in Table 4.^{**} When ages are calculated from the potassium and argon measurements, the variation attributed to experimental factors disappears.

Table 4 separates the contribution of sampling and laboratory differences to the variances for potassium and argon measurements. Because variability within each of the four sites is similar, only overall estimates are shown. Included in Table 4 are the standard deviations and confidence intervals for potassium and argon measurements as well as age calculations.

Each laboratory performed at least two measurements of potassium and argon content of each rock sample. Table 5 lists the average of these subsample or aliquot measurements. The estimated contribution of subsample variance to overall sample-to-sample variance is shown in Table 6. Subsample variation contributes little to the total sampling variation of potassium measurements, but for two of the three laboratories, it contributes substantially to the variance among argon measurements.

^{*}Satterthwaite's approximation (Graybill, 1961, p 369) was used to obtain approximate degrees of freedom associated with the estimated σ 's in Table 4. Note that the standard error in Table 4 is about twice the corresponding standard error in Table 3, but widths of confidence intervals are not increased by the same factor. This occurs because standard errors in Table 4 (estimated σ) are based on more degrees of freedom and hence are more precisely defined than those in Table 3.

^{**}In the analysis of variance for potassium and argon data, variations associated with sample collections and with interactions among sites, laboratories, and collections were pooled to obtain the variation associated with "experimental factors." There are thus two levels of random variation in the data: variation among groups of samples and variation among samples within a group. For age calculations, though, the variation among sample groups was negligible.

Table 3. Average Reported Ages, Standard Errors, Confidence Intervals, and Sources of Variance for Each Site in Crater Flat

	Site 1	Site 2	Site 3	Site 4	Overall*
Average Age Est (my)	0.46	1.41	3.96	3.97	—
Std Error of Est (my)	0.20	0.14	0.16	0.15	0.16
90% Confidence Interval on "True Age"*** (my)	±0.58	±0.41	±0.47	±0.44	±0.47
95% Confidence Interval on "True Age"*** (my)	±0.86	±0.60	±0.69	±0.65	±0.69
Variance Estimates (my)					
Sampling	0.018	0.062	0.081	0.010	0.044
Laboratory	0.113	0.049	0.061	0.067	0.071
Total	0.131	0.112	0.142	0.078	0.115

*Apparent differences among site variance estimates could be "random" allowing data to be combined to provide overall values.

**Based on a set of 18 samples composed of six samples from each of the three laboratories.

Table 4. Variance, Standard Deviation (σ), and Confidence Intervals for Potassium and Radiogenic Argon Measurements and Age Calculations for All 72 Samples

	Potassium Analysis	Argon Analysis	Age Estimates
<i>Source of Variation</i>			
Sampling	0.0026 (%) ²	0.325 (mol/g x 10 ⁻¹²) ²	0.044 (10 ⁶ yr) ²
Experimental Factors	0.0051 (%) ²	0.249 (mol/g x 10 ⁻¹²) ²	0.000 (10 ⁶ yr) ²
Laboratory	0.0024 (%) ²	0.204 (mol/g x 10 ⁻¹²) ²	0.071 (10 ⁶ yr) ²
Total*	0.0101 (%) ²	0.778 (mol/g x 10 ⁻¹²) ²	0.115 (10 ⁶ yr) ²
Estimated σ	0.10%	0.88 mol/g x 10 ⁻¹²	0.34 x 10 ⁶ yr
Degrees of Freedom**	15	18	5
90% Confidence Interval on "True Value"†	±0.18%	±1.53 mol/g x 10 ⁻¹²	±0.68 x 10 ⁶ yr
95% Confidence Interval on "True Value"†	±0.21%	±1.85 mol/g x 10 ⁻¹²	±0.87 x 10 ⁶ yr

*Total variance is for a single sample measured by a single randomly selected laboratory.

**"Degrees of freedom" is a parameter used in calculating confidence limits on σ .

†For an age of one sample determined by a single laboratory; the "true" age is within the given interval relative to appropriate quantities reported in Tables 1 and 5.

Table 5. Reported Potassium and Argon Analyses of Crater Flat Basalts

Sample Set	Potassium (%)			Radiogenic ⁴⁰ Argon (mol/g x 10 ⁻¹²) Parentheses Indicate % Atmospheric Argon					
	Laboratory A ¹	Laboratory B ¹	Laboratory C ¹	Laboratory A ⁴	Laboratory B ⁴	Laboratory C ⁴	Laboratory A ⁴	Laboratory B ⁴	Laboratory C ⁴
Site 1	1	1.389	1.633	1.625 ²	1.75 (96.5)	0.23 (98.4)	1.69 (92.1) ⁶		
	2	1.528	1.606	1.643 ²	1.78 (98.5)	0.10 (99.9)	1.74 (96.0) ⁶		
	3	1.518	1.628	1.580 ²	2.10 (97.2)	-0.08 (100.0)	1.80 (93.5) ⁶		
	4	1.611	1.545	1.597 ²	1.70 (98.4)	0.21 (98.9)	1.54 (92.8) ⁶		
	5	1.586	1.577	1.607 ²	3.25 (97.6)	0.30 (99.6)	1.64 (96.6) ⁶		
	6	1.503	1.558	1.566	1.58 (97.7) ⁹	0.48 (99.1)	1.05 (93.4) ⁶		
Site 2	7	1.493	1.472	1.473 ³	4.60 (94.1)	2.46 (94.6)	3.74 (83.6)		
	8	1.446	1.380	1.459 ³	4.56 (95.6)	2.27 (96.4)	4.44 (90.8) ⁶		
	9	1.491	1.471	1.443	4.00 (98.0)	2.48 (91.6)	3.51 (87.6) ⁶		
	10	1.388	1.519	1.414	4.55 (97.1)	4.39 (98.5)	3.95 (92.0) ⁶		
	11	1.391	1.404	1.397 ²	2.48 (96.8)	2.63 (97.9)	3.98 (96.0) ⁶		
	12	1.367	1.408	1.437 ²	3.68 (96.7)	2.71 (96.2)	9.12 (69.9) ^{6,10}		
Site 3	13	1.272 ⁴	1.710 ⁴	1.574	10.75 (90.8)	10.73 ⁶ (55.4) ⁸	10.54 (50.7) ⁶		
	14	1.287 ⁴	1.555	1.460 ²	9.80 (88.3)	10.35 (52.0)	9.91 (94.8) ⁷		
	15	1.249	1.680	1.514 ²	8.08 (93.0)	10.95 (54.6)	10.49 (56.9) ⁶		
	16	1.309	1.632	1.572 ²	10.93 (91.9)	10.55 (45.5)	10.30 (87.1) ⁶		
	17	1.344	1.416	1.457 ²	10.43 (83.3)	8.95 (85.6)	10.48 (57.7) ⁶		
	18	1.342	1.465	1.409 ²	9.40 (89.5)	9.45 (60.3)	3.45 (95.4) ^{6,10}		
Site 4	19	1.394	1.543	1.387	10.65 (77.7)	10.10 (74.3)	9.61 (33.5) ⁶		
	20	1.470	1.452	1.309 ²	10.93 (75.5)	9.55 (52.3)	9.08 (56.4) ⁶		
	21	1.399	1.591	1.421	10.40 (66.6)	9.75 (41.5)	10.22 (32.8) ⁶		
	22	1.530	1.436	1.431 ²	11.35 (75.5)	9.10 (68.2)	9.99 (52.9)		
	23	1.269	1.434	1.437 ²	9.65 (81.8)	9.15 (64.4)	9.39 (47.9) ⁶		
	24	1.250	1.366	1.385 ²	9.08 (75.6)	8.75 (60.1)	9.85 (65.5) ⁶		

¹Average of 2 separate analyses, rounded upward from 5 unless indicated by other footnote

²Average of 3 separate analyses, rounded upward from 5

³Average of 4 separate analyses, rounded upward from 5

⁴Average of 2 analyses, rounded upward from 5 unless indicated by other footnote

⁵Average of 3 analyses, rounded upward from 5

⁶Average of 4 analyses, rounded upward from 5

⁷Average of 5 analyses, rounded upward from 5

⁸Average of 6 analyses, rounded upward from 5

⁹Only 1 analysis reported or legible on report sheets

¹⁰Apparently labels for samples 12(c) and 18(c) were interchanged.

Table 6. Variance Estimates of Potassium and Argon Measurements for Subsamples and Samples

Variance	Laboratory A	Laboratory B	Laboratory C
Potassium			
Sample	.0032	.0030	.0017
Subsample	.00041	.00016	.00004
Contribution of Subsample*	6.4%	2.7%	1.2%
Argon			
Sample	.547	.250	.178
Subsample	.494	.119	.025
Contribution of Subsample*	45%	24%	7%

*Divide subsample variance by two to obtain its approximate contribution to total sample variance, because generally two subsamples were analyzed for each rock sample.

The results of this experiment support the contention of others that ^{40}K - ^{40}Ar age determinations must be carefully interpreted in terms of their relation to true ages (Holmes, 1962; Damon, 1970; Dalrymple and Lanphere, 1969, 1974; Berger and York, 1970; Noble and Naughton, 1968; Giletti, 1971; McDougall, 1971, among others).

Possible Sources of Uncertainty

It is generally accepted in the geological sciences that uncertainty associated with the "true" age of a rock is commonly greater than the uncertainty associated with analytical precision, as reported by geochronologists. In pursuing the sources of this larger uncertainty, much attention has focused on leakage or assimilation of radiogenic argon from or into rock systems before or after the start of the radiometric clocks (Damon et al, 1967; Baksi, 1973; Krummenschacher, 1970; Shafiqullah and Damon, 1974; Brewer, 1969; McDougall et al, 1979; Dalrymple and Lanphere, 1974; Dalrymple, 1969; and York et al, 1969, among others). Generally, such discussions are concerned with lithologic heterogeneity on scales ranging from intracrystalline to the entire rock mass. Differential preservation of either potassium or argon in the crystallized rock as well as the evolution and character of the initial rockforming magma can contribute to real

differences among K-Ar ratios from even a single lava flow. This, in turn, can lead to variations in age determinations of a crystallizing event.

Another source of variation in radiometric age determinations is the difference in analytical methods and instruments used by various geochronology laboratories. Kuntz et al (1980) discuss these sources of age discrepancies for young basalts in detail. Variance among and within the subsamples and the overall laboratory-to-laboratory differences observed in this study supports previous conclusions that laboratory techniques contribute significantly to limits on the reproducibility for measurements of potassium and especially argon contents of young basalts.

A small source of variation may be attributed to the use of different numerical values for electron and beta potassium decay constants. One laboratory in this study used 4.72×10^{-10} per year for $\lambda\beta$ and 0.585×10^{-10} per year for $\lambda\epsilon$, whereas the other two laboratories used 4.96×10^{-10} per year and 0.581×10^{-10} per year for $g\beta$ and $\lambda\epsilon$, respectively. However, these differences caused negligible variation among the reported ages.

Isochron plots (Hayatsu and Carmichael, 1970; Shafiqullah and Damon, 1974) provide a method for estimating corrections for extraneous argon. This method must still rely on measured values for potassium and argon and does not explain the variance in these values.

From the perspective of an independent user of K-Ar ages, any of the possible lithologic or analytical sources of variance could be responsible for introducing error to age determinations. It is beyond the scope of this study to evaluate which factor or combination of factors can be applied to obtain corrections for the reported ages. Therefore, equal credibility is assumed for each reported analysis. The variability among reported ages is treated statistically as a normally distributed population about a true mean. The statistical analysis leads to a set of age brackets that can be assigned with specified confidence levels to each site. The standard deviation of ages reported for each site and the corresponding confidence intervals are appropriate measures of the uncertainty associated with K-Ar ages of these young basalts.

Conclusions

The following conclusions are based on the results of this study:

1. Quaternary basalts with about 1.5% potassium content can be assigned, at 90% confidence, an age within an interval of about 1 my if six

samples from a single site are radiometrically dated by ^{40}K - ^{40}Ar methods by each of three laboratories.

2. Wider intervals are required for the same degree of confidence for an age determined by a single laboratory for a single sample.
3. Standard precision brackets that commonly accompany reported K-Ar ages for young basalts do not adequately represent the uncertainty inherent in the ages.
4. Geomorphic and stratigraphic methods are better than K-Ar dating techniques for determining the relative age of Quaternary basalts because the accuracy of K-Ar methods prohibits confident resolution within the past million or so years.

Recommendations

The following recommendations reflect user concerns and are offered for consideration by the community of geochronologists.

1. Statistical means and standard deviations for potassium, radiogenic argon, and atmospheric argon contents and radiometric ages of numerous basalt deposits whose mean radiometric ages span the Quaternary period should be established as standards for K-Ar age determinations of Quaternary basalts. Statistical parameters for standard deposits should be determined by combining results from several independent laboratories that perform redundant analyses on multiple samples. The standards should be determined and the results published by some central organization, preferably the National Bureau of Standards. Current standards for radiometric dating of rocks, if available at all, are commonly specific minerals with very narrow ranges in composition. This type of standard is well suited for calibrating instruments and determining precision but not well suited for assessing the accuracy of the

age of a rock that is of a class with a wide range in composition. This recommendation addresses a means of establishing accuracy standards to compliment existing precision standards. Similar standards for other time periods and rock types may also be desirable, but the results of this study are restricted to Plio-Pleistocene basalts.

Samples from the deposits upon which the standards are based should be available to individual analysts for calibration of their results during study of the radiometric ages of young basalts. Results of individual analyses on the calibration samples should be reported to the organizing institution for incorporation in the evolving statistical standards for the deposits.

2. The practice of reporting precision of radiometric ages for young basalts to the nearest tens of thousands of years should be abandoned because the precision, as reported, is misleading. Rather, precision should be reported for individual potassium and argon measurements, and confidence intervals based on statistical standards as recommended above should be reported for ages.
3. Stratigraphic and geomorphic interpretations of relative ages of Quaternary basalts should not be modified to fit radiometric age distributions without careful consideration of the real uncertainty in the radiometric ages.
4. A set of experiments should be designed to assess the dependence of K-Ar age uncertainties for young basalts on each of the components of lithologic and analytical variations. Data from the study reported here could be analyzed in this manner as a step in solving the problem of accuracy for K-Ar ages of Quaternary basalts. Time and budgets have precluded carrying this study to its fullest extent; therefore, the results were presented at a stage of development thought sufficient to illustrate the distinction between precision and accuracy.

Bibliography

- Baksi, A. K., "K-Ar Dating — Loading Techniques in Argon Extraction Work and Sources of Air Argon Contamination," *Can J Earth Sci*, 1973, 10, 1678-1684.
- Berger, G. W. and D. York, "Precision of the $^{40}\text{Ar}/^{39}\text{Ar}$ Dating Technique," *Earth Planet Sci Lett*, 1970, 9, 39-44.
- Brewer, M. S., "Excess Radiogenic Argon in the Metamorphic Micas From the Eastern Alps, Austria," *Earth Planet Sci Lett*, 1969, 6, 321-331.
- Dalrymple, G. B., " $^{40}\text{Ar}/^{36}\text{Ar}$ Analyses of Historic Lava Flows," *Earth Planet Sci Lett*, 1969, 6, 47-55.
- Dalrymple, G. B. and M. A. Lanphere, *Potassium-Argon Dating: Principles, Techniques and Application to Geochronology*, 1969, 258 pp, W. H. Freeman.
- Dalrymple, G. B. and M. A. Lanphere, " $^{40}\text{Ar}/^{39}\text{Ar}$ Age Spectra of Some Undisturbed Terrestrial Samples," *Geochim Cosmochim Acta*, 1974, 38, 715-738.
- Damon, P. E., A. W. Laughlin, and J. K. Percious, "Problem of Excess Argon-40 in Volcanic Rocks, *Radioactive Dating and Methods of Low-Level Counting*" (Vienna: Int Atomic Energy Agency 1967), 463-481.
- Damon, P. E., "A Theory of 'Real' K-Ar Clocks," *Eclogae Geol Helv*, 1970, 63, 69-76.
- Giletti, B. J., "Discordant Isotopic Ages and Excess Argon in Biotites," *Earth Planet Sci Lett*, 1971, 10, 157-164.
- Graybill, F. A., 1961, *An Introduction to Linear Statistical Models*, Vol 1 (New York: McGraw Hill, 1971).
- Hayatsu, A. and C. M. Carmichael, "K-Ar Isochron Method and Initial Argon Ratios," *Earth Planet Sci Lett*, 1970, 8, 71-76.
- Holmes, A., "Absolute Age - A Meaningless Term," *Nature*, 1962, 196, 1238.
- Krummenacher, D., "Isotopic Composition of Argon in Modern Surface Volcanic Rocks," *Earth Planet Sci Lett*, 1970, 8, 109-117.
- Kuntz, M. A., D. B. Dalrymple, D. E. Champion, and D. J. Doherty, *An Evaluation of Potential Volcanic Hazards at the Radioactive Waste Management Complex, Idaho National Engineering Laboratory, Idaho*, USGS Open File Report 80-388, 1980.
- McDougall, I., H. A. Polach, and J. J. Stipp, "Excess Radiogenic Argon in Young Subaerial Basalts From Auckland Volcanic Field, New Zealand," *Geochim Cosmochim Acta*, 1969, 33, 1485.
- McDougall, I., "The Geochronology and Evolution of the Young Volcanic Island of Reunion, Indian Ocean," *Geochim Cosmochim Acta*, 1971, 35, 261-289.
- Noble, C. S. and J. J. Naughton, "Deep Ocean Basalts: Inert Gas Content and Uncertainties in Age Dating," *Science*, 1968, 162, 265-267.
- Shafiqullah, M. and P. E. Damon, "Evaluation of K-Ar Isochron Methods," *Geochim Cosmochim Acta*, 1969, 38, 1341-1358.
- York, D., R. M. MacIntyre, and J. Gittins, "Excess Radiogenic ^{40}Ar in Cancrinite and Sodalite," *Earth Planet Sci Lett*, 1969, 7, 25-28.

DISTRIBUTION:

TIC-4500-R70 UC-70 (323)

**US Department of Energy (5)
Office of Waste Isolation
NE-22
Germantown, MD 20767
Attn: W. W. Ballard, Jr., Director
 J. W. Bennett
 C. R. Cooley, Team Leader
 Technology Development Team
 J. J. Fiore
 C. H. George, Team Leader,
 Siting Team**

**US Department of Energy
Office of Terminal Waste Disposal &
Remedial Action Nuclear Energy
NE-20
Germantown, MD 20767
Attn: F. E. Coffman, Acting Director**

**US Department of Energy
Repository Projects Team
NE-22
Germantown, MD 20767
Attn: R. Stein, Team Leader**

**US Department of Energy
Projects & Facilities Management
Richland Operations Office
Richland, WA 99352
Attn: H. J. Anttonen, Asst Manager**

**US Nuclear Regulatory Commission (3)
Division of Waste Management
Washington, DC 20555
Attn: Chief, High-Level Waste Technical
 Development Branch
 NTS Project Manager (2)**

**US Department of Energy
National Waste Terminal
Storage Program Office
505 King Ave
Columbus, OH 43201
Attn: J. O. Neff, Program Manager**

**Battelle (9)
Office of Nuclear Waste Isolation
505 King Ave
Columbus, OH 43201
Attn: N. E. Carter
 S. Goldsmith
 G. Heim
 B. Madia
 ONWI Library (5)**

**Battelle (2)
Office of NWTs Integration
505 King Avenue
Columbus, OH 43201
Attn: W. A. Carbiener
 J. O. DuGuid**

**Los Alamos National Laboratory (3)
University of California
PO Box 1663
Los Alamos, NM 87545
Attn: B. M. Crowe, MS 329
 D. T. Oakley, Technical
 Project Officer, MS F-671
 O. C. Hoffman, MS 760**

**Rockwell International Atomics (2)
International Division
Rockwell Hanford Operations
Richland, WA 99352
Attn: R. Deju
 G. Hunt**

**Governor's Office of Planning Coordination
State of Nevada
Capitol Complex
Carson City, NV 89023
Attn: R. M. Hill, State Planning Coordinator**

**Department of Energy
State of Nevada
Capitol Complex
Carson City, NV 89710
Attn: S. A. Robinson**

DISTRIBUTION (cont):

Lawrence Livermore National Laboratories (3)
University of California
PO Box 808, MS L-204
Livermore, CA 94550
Attn: L. D. Ramspott,
 Technical Project Manager, MS L-204
 A. J. Rothman, MS L-204
 K. Street, Jr., MS L-209

US Geological Survey (4)
PO Box 25046
Federal Center
Denver, CO 80225
Attn: W. W. Dudley, Jr.
 Technical Project Officer, MS 416
 R. J. Marvin, Branch of Isotope Geology
 G. L. Dixon, Special Projects Group, MS 954
 W. J. Carr, Special Projects Group, MS 954

W. S. Twenhofel
820 Estes St
Lakewood, CO 80215

US Department of Energy (15)
PO Box 14100
Las Vegas, NV 89114
Attn: B. W. Church, Director,
 Health Physics Division
 D. A. Nowack (8)
 D. L. Veith, Director,
 Waste Management Project Office (5)
 D. F. Miller, Director,
 Office of Public Affairs

Holmes & Narver, Inc
PO Box 14340
Las Vegas, NV 89114
Attn: A. E. Gurrola

Reynolds Electrical & Engineering Co., Inc
PO Box 1440, MS 555
Las Vegas, NV 89114
Attn: H. D. Cunningham

Fenix & Scisson, Inc
PO Box 15408
Las Vegas, NV 89114
Attn: J. A. Cross

Westinghouse - AESD
PO Box 708, MS 703
Mercury, NV 89023
Attn: A. R. Hakl, Site Manager

US Department of Energy (2)
Technical Information Center
PO Box 62
Oak Ridge, TN 37830

University of Arizona (2)
Laboratory of Isotope Geochemistry
Tucson, AZ 85721
Attn: P. E. Damon
 M. Shafigullah

Krueger Enterprises, Inc.
Geochron Laboratories Division
24 Blackstone Street
Cambridge, MA 02139
Attn: H. W. Krueger

University of California, Berkeley (2)
Department of Geology and Geophysics
Berkeley, CA 94720
Attn: G. H. Curtis
 R. Drake

1540 W. C. Luth
7200 J. M. Wiesen
7220 J. M. Wiesen, Actg
7223 R. G. Easterling (10)
7223 R. R. Prairie
7254 F. W. Muller
7254 G. F. Rudolfo
9000 G. A. Fowler
9413 R. L. Hunter
9700 E. H. Beckner
9730 W. D. Weart
9760 R. W. Lynch
9761 L. W. Scully
9762 L. D. Tyler
9763 A. R. Lappin
9763 J. R. Tillerson
9764 J. T. Neal
9764 A. E. Stephenson
9764 S. Sinnock (20)
8214 M. A. Pound
3141 L. J. Erickson (5)
3151 L. W. Garner (3)

Hydraulic Fracturing Stress Measurements at Yucca Mountain, Nevada, and Relationship to the Regional Stress Field

J. M. STOCK,¹ J. H. HEALY, S. H. HICKMAN,¹ AND M. D. ZOBACK²

Office of Earthquakes, Volcanoes, and Engineering, U.S. Geological Survey, Menlo Park, California

Hydraulic fracturing stress measurements and acoustic borehole televiewer logs were run in holes USW G-1 and USW G-2 at Yucca Mountain as part of the Nevada Nuclear Waste Storage Investigations for the U.S. Department of Energy. Eight tests in the saturated zone, at depths from 646 to 1288 m, yielded values of the least horizontal stress S_3 that are considerably lower than the vertical principal stress S_2 . In tests for which the greatest horizontal principal stress S_1 could be determined, it was found to be less than S_2 , indicating a normal faulting stress regime. The borehole televiewer logs showed the presence of long (in excess of 10 m), vertical, drilling-induced fractures in the first 300 m below the water table. These are believed to form by the propagation of small preexisting cracks under the excess downhole fluid pressures (up to 5.2 MPa) applied during drilling. The presence of these drilling-induced hydrofractures provides further confirmation of the low value of the least horizontal stresses. A least horizontal principal stress direction of N60°W-N65°W is indicated by the orientation of the drilling-induced hydrofractures (N25°E-N30°E), and the orientation of stress-induced well bore breakouts in the lower part of USW G-2 (N65°W). This direction is in good agreement with indicators of stress direction from elsewhere at the Nevada Test Site. The observed stress magnitudes and directions were examined for the possibility of slip on preexisting faults. Using these data, the Coulomb criterion for frictional sliding suggests that for coefficients of friction close to 0.6, movement on favorably oriented faults could be expected. For coefficients of friction of 1.0, preexisting faults of all orientations should be stable. Laboratory studies on the Yucca Mountain tuffs, reported elsewhere, yield coefficients of friction ranging from 0.6 to 0.9.

INTRODUCTION

In an area such as Yucca Mountain, Nevada Test Site, where a nuclear waste repository might be constructed [Winoograd, 1981], a knowledge of the stress field is needed for the proper design of the repository and the evaluation of seismic stability and likelihood of motion on preexisting faults. Activities related to the construction and use of a nuclear waste repository, such as drilling and excavation, as well as the generation of heat by the stored waste, will change the local stress field to some degree. The magnitude of these changes can be estimated, but a knowledge of the preexisting tectonic stresses and their orientations is vital to prediction of how these additional imposed stresses will affect the tectonic stability of the repository area.

Previous workers have obtained a great deal of information about stress magnitudes and orientations in the Nevada Test Site (NTS) area. These data, summarized in part by Carr [1974] and Zoback and Zoback [1980], show that the NTS region currently exhibits both normal and strike-slip faulting, with a least horizontal principal stress direction varying from NW to WNW. Much of this stress information is poorly constrained; direct measurement of the current tectonic stress field using hydraulic fracturing and overcoring techniques had only been obtained at Rainier Mesa, in the northern part of NTS, about 40 km NNE of Yucca Mountain [Haimson et al., 1974; Smith et al., 1981; Ellis and Magner, 1980]. In order to determine the magnitudes and directions of the principal stresses at the proposed repository site, we performed a series

of hydraulic fracturing stress measurements and acoustic borehole televiewer observations in two wells (USW G-1 and USW G-2).

LOCATION AND GEOLOGIC SETTING

Yucca Mountain straddles the western boundary of the Nevada Test Site at approximate coordinates 36°50'N, 116°28'W (Figure 1). It is bounded on three sides by alluvial areas of low relief: on the east by Jackass Flats, on the west by Crater Flat, and on the south by the Amargosa valley.

Yucca Mountain consists of a series of gently east tilted blocks of Miocene volcanic units. The Tiva Canyon member of the Paintbrush Tuff (pre-11 Ma [Marvin et al., 1970]) crops out over most of the surface. Stratigraphic units encountered below the Tiva Canyon member, in descending order, are Yucca Mountain member, Pah Canyon member, and Topopah Springs member of the Paintbrush Tuff; the tuffaceous beds of Calico Hills; the Prow Pass member, Bullfrog member, and Tram member of the Crater Flat Tuff; lava and flow breccia; and the Lithic Ridge Tuff. Minor bedded tuffs are locally present between each of these units.

Drilling, gravity, and seismic refraction data show that the Miocene volcanic units probably extend to at least 3000 m depth beneath most of Yucca Mountain [Snyder and Carr, 1984; Hoffman and Mooney, 1983]. However, a gravity high on the east side of Yucca Mountain is believed to correspond to a high in the prevolcanic surface. In this area, drill hole Ue25p-1 (see Figure 2) penetrates Silurian limestones and dolomites at 1400 m depth. These Paleozoic rocks are part of the Precambrian through upper Paleozoic clastic and carbonate sequence that crops out west of Crater Flat at Bare Mountain and east of Yucca Mountain in the Calico Hills and Striped Hills.

The structural style at Yucca Mountain is dominated by high-angle, NW to NE striking, west dipping normal faults which tilt strata to the east (Figure 2). Vertical offset on these west dipping faults is generally small except for along the

¹ Now at Department of Earth, Atmospheric, and Planetary Sciences, Massachusetts Institute of Technology, Cambridge.

² Now at Department of Geophysics, Stanford University, California.

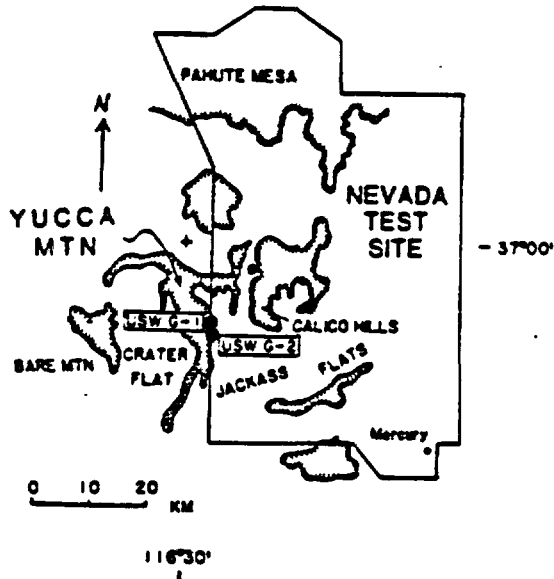


Fig. 1. Map of the Nevada Test Site and vicinity, showing locations of Yucca Mountain, Crater Flat, Pahute Mesa, Bare Mountain, and Jackass Flats.

bounding faults (e.g., the Paintbrush Canyon fault, with approximately 500 m vertical offset [Scott and Bonk, 1984]). The major normal movement on these faults occurred between 13 and 11.5 Ma; minor normal, strike-slip, or oblique movement may have continued into the Pliocene [Scott and Castellanos, 1984]. A second style of vertical NW striking faults, with sub-horizontal slickensides and offsets of 100 m or less, is also present; motion on these faults is believed to predate 11.5 Ma [Scott and Castellanos, 1984].

Crater Flat, a broad low region of alluvium and some Quaternary basalt eruptive centers, lies immediately west of Yucca Mountain. The volcanics of Crater Flat have been divided into three groups: 3.7-Ma basalt, consisting of feeder dikes, scoria deposits, and lava flows in the southeast portion of Crater Flat; a series of four 1.1-Ma Strombolian cinder cones along a slightly arcuate trend through the center of Crater Flat; and the 0.3-Ma Lathrop Wells cinder cone, immediately south of Yucca Mountain [Vaniman and Crowe, 1981]. Drill holes VH-1 and VH-2 in central Crater Flat pass through alluvium, Paleozoic slide blocks, and the Timber Mountain Tuff and encounter the same Miocene volcanic units seen in drill holes at Yucca Mountain [Carr, 1982, and written communication, 1984]. The dominant structural style of east tilted blocks bounded by west dipping high-angle faults extends from Yucca Mountain into eastern Crater Flat. Such faults have caused over 550 m of vertical separation in the Paintbrush Tuff between drill holes VH-1 and VH-2; they also produce minor displacement in the 3.7-Ma volcanics [Carr, 1982].

USW G-1 is located in Drill Hole Wash, on the east side of Yucca Mountain, at coordinates 36°52'00"N, 116°27'30"W, and a surface elevation of 1326 m. USW G-2 is east of the crest of Yucca Mountain, at coordinates 36°53'22"N, 116°27'35"W. Its surface elevation is 1554 m. Projections of the two holes along lines of maximum topographic relief (Figure 3) show that G-1 has significant drift toward the southwest into Yucca Mountain, whereas G-2 is essentially vertical. The holes penetrate units ranging from the Tiva Canyon member of the Paintbrush Tuff to some unnamed

tuffs below the Lithic Ridge Tuff (see Spengler et al. [1981] and Maldonado and Koether [1983] for detailed stratigraphic descriptions).

HYDRAULIC FRACTURING PROCEDURES

The hydraulic fracturing stress measurement technique has been extensively described elsewhere [e.g., Haimson and Fairhurst, 1967; Hickman and Zoback, 1983]. Briefly, an interval of the drill hole is isolated between two rubber packers and pressurized until a tensile fracture forms in the borehole wall. The test interval is then "shut-in" (sealed off at the surface) and its pressure-time behavior is monitored. The pressure at which the fracture closes away from the well bore usually appears as an inflection in the pressure-time curve just after shut-in and is referred to as the instantaneous shut-in pressure, or ISIP. The surface valve is then opened to allow the pressure to bleed back to its pretest value. Normally, several more cycles of pressurization, shut-in, and bleeding back are conducted, until the ISIP reaches a stable value; this is interpreted as the normal stress on the fracture away from the well bore [Hickman and Zoback, 1983]. Theory [Hubbert and Willis, 1957] and numerous laboratory experiments [Haimson and Fairhurst, 1970; Haimson and Avasthi, 1975] show that the hydraulic fracture should propagate in a direction perpendicular to the direction of the least horizontal principal stress S_H , and thus the ISIP is taken to be equal to S_H .

The magnitude of the maximum horizontal principal stress S_H can be determined if the rock is assumed to be homogeneous, isotropic, and linearly elastic, with one principal stress direction parallel to the borehole axis (i.e., vertical). Under these conditions the minimum tangential stress at the borehole wall occurs at the azimuth of the greatest horizontal principal stress S_H . The interval pressure required to create a hydraulic fracture at this azimuth depends on the tensile strength T and the pore pressure P_p , and is called the breakdown pressure P_b [Haimson and Fairhurst, 1967; after Hubbert and Willis, 1957]:

$$P_b = 3S_v - S_H + T - P_p \quad (1)$$

If an ISIP is not visible on the pressure-time curve (for example, because the high permeability of the interval obscures the inflection point), a step rate injection test [Earlougher, 1977] can help to constrain the normal stress on the fracture [see Hickman et al., 1985]. The stable pumping pressure for each of a series of decreasing flow rates is recorded. The resulting plot of flow rate as a function of pumping pressure will generally be linear in two regions, with a slope change reflecting the decrease in apparent permeability of the interval as the fracture closes.

Values of S_v and P_p determined from hydraulic fracturing test records can be used in equation (1) to solve for S_H if the values of T and P_p are known. Because tensile strength T is observed to depend on both the sample size and the type of tensile strength test performed [e.g., Hudson, 1971; Ratigan, 1983], T as a function of sample size must be obtained through careful laboratory work and then extrapolated upward to the in situ borehole size. A more reliable value of S_H can be obtained by using the fracture reopening pressure on the second cycle (P_r at $T = 0$) to eliminate T from equation (1) [Bredenhoefst et al., 1976]:

$$P_r(T = 0) = 3S_v - S_H - P_p \quad (2)$$

Equation (2) is only valid if the excess fluid pressure can be bled back from the interval after each cycle, so that the equi-

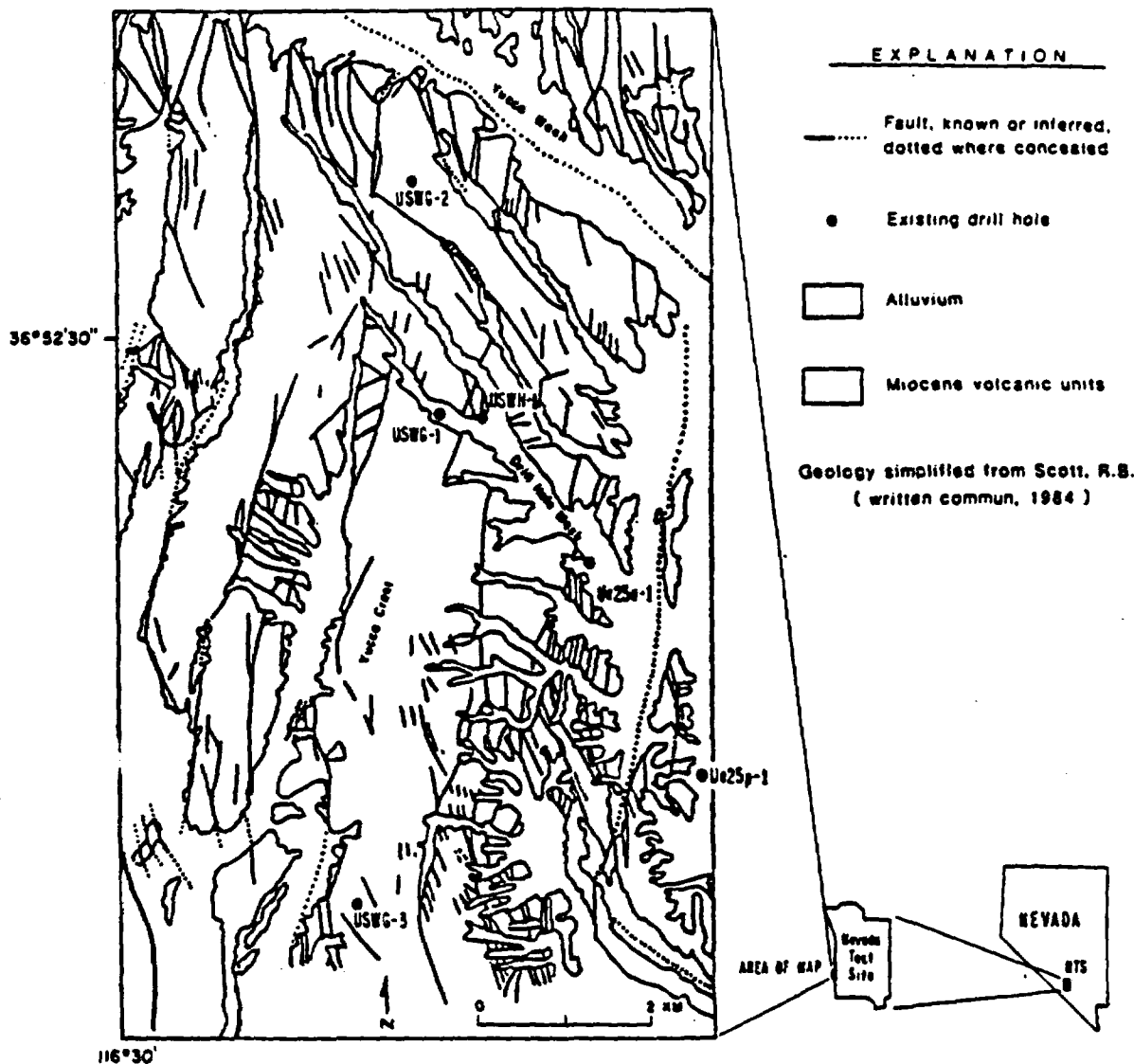


Fig. 2. Map of Yucca Mountain showing locations of drill holes discussed in text. White is outcrop of volcanics, and stippled pattern represents alluvium.

librium pore pressure of the wall rock is not significantly disturbed. If the pressure in the interval cannot be bled back, the higher pressure in the interval may raise the pore pressure in the rock around the hole. Use of the equilibrium value of P_p in equation (2) will then result in an erroneously high value of S_H . Under these circumstances, equation (2) can only be used to place an upper limit on the value of S_H [Hickman and Zoback, 1983]. In this report we rely primarily on equation (2) for determination of S_H values. The uncertainties in these S_H values due to possible changes in P_p are discussed along with the S_H results below.

After successful hydraulic fracturing tests, impression packers are often used to obtain an oriented impression of the hydraulic fracture and determine the S_3 direction. In the tests in USW G-1 and USW G-2, no impression packers could be run due to time constraints. However, consistent and detailed information on the S_3 direction was obtained from other features in the televiwer log discussed below.

HYDRAULIC FRACTURING RESULTS

Eleven successful hydraulic fracturing tests were conducted in USW G-1 and USW G-2 (Table 1; Figures 4 and 5). The

three shallowest tests in USW G-2 were in the unsaturated zone; all other tests were below the water table.

The unusually low water levels in these holes (575 m in USW G-1 and 526 m in USW G-2) and the low horizontal stresses encountered in the tests mandated some modifications of typical testing procedure. The pressure in the interval often fell below surface hydrostatic pressure during the tests. In addition to the mechanical pressure recorder normally used downhole, a downhole electronic transducer transmitted pressure data to the surface through the wireline to provide real-time information on interval pressure. Because a wireline lubricator was used at the surface to seal the wellhead against the wireline, the rate of pressure decay decreases considerably whenever the pressure in the interval falls below surface hydrostatic pressure (e.g., Figure 5; see also Stock et al. [1984]). This change in slope is not necessarily an ISIP; it is caused by the change in compliance of the fluid-filled drill pipe and packer system as the water level drops below the top of the tubing string and a two-phase (water plus low-pressure water vapor) system is created. This transition from a fluid-filled (low compliance) to fluid- and vapor-filled (high compliance) system is reflected by a sudden increase in the apparent bore-

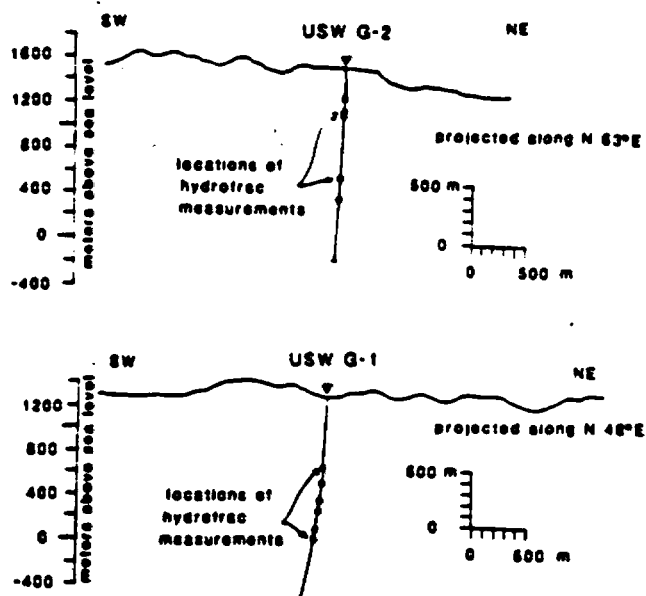


Fig. 3. Projections of holes USW G-1 and USW G-2 against topography, showing depths to hydrofract measurements.

hole storage coefficient. (See Cooper et al. [1967] and Bredehoeft and Papadopoulos [1980] for a discussion of borehole storage effects related to in situ permeability tests.)

The eight tests below the water table had clear breakdown pressures, and values of S_h were determined from stable ISIP values or flat pumping pressures (Table 1). For three of the tests in USW G-2, step rate injection tests on the final pump-

ing cycles were used to further constrain the ISIP values (Figure 5 and Stock et al. [1984]). In the three tests in the unsaturated zone (tests at 295, 418, and 432 m, USW G-2, Figure 5) the breakdown pressures on the first cycle were the same as fracture reopening pressures on the later cycles, suggesting that preexisting fractures were being reopened rather than new hydrofractures being created. If the preexisting fractures were not perpendicular to S_h , the normal stress on the fracture (the ISIP) may exceed S_h . We therefore use the three ISIP values recorded in these tests as upper bounds on the S_h value at these depths. Because no televiewer logs or fracture impressions could be obtained in the unsaturated zone, information on density and orientation of preexisting fractures is poor. However, as discussed below, most of the fractures in the zone below the water table in USW G-2 have normals within 30° of the S_h direction. If the fractures in the unsaturated zone have similar orientations, it is likely that the ISIP values determined from these tests are close to S_h .

Because of uncertainty over which values of tensile strength to use in equation (1), estimates of the maximum horizontal stress S_H are obtained using equation (2). These S_H values are poorly constrained because of the following uncertainties in P_p . In USW G-1 the circulation valve between the packers was opened using a weighted bar on the end of the wireline. This bar had to be brought back to the surface prior to sending the pressure gauge downhole and sealing off the wellhead so that testing could begin. This required a wait of approximately 1 hour between the time that the circulation valve between the packers was opened (allowing water pressure in the drill pipe to enter the test interval) and the time that pressurization of the interval to breakdown could begin.

TABLE 1. Summary of Stress Measurements, USW G-1 and USW G-2

Depth, m	Hydraulic Fracturing Data				Principal Stresses			Comments
	Breakdown Pressure, MPa	Shut-In Pumping Pressure, MPa	Hydrostatic Pressure, MPa	Pore Pressure,*† MPa	Minimum Horizontal Stress, MPa	Vertical Stress, MPa*		
					USW G-1			
646	8.3	4.2 ± 0.2	6.2	0.7	4.2 ± 0.2	12.9	Minimum horizontal stress from flat subhydrostatic pumping pressure attained during second cycle. S_h may thus be several bars too high due to pressure gradient in fracture.	
792	10.2	7.2 ± 0.2	7.9	2.2	7.2 ± 0.2	15.9	Same as above.	
945	13.2	9.0 ± 0.2	9.2	3.6	9.0 ± 0.2	19.2	Same as above.	
1038	13.5	10.6 ± 0.2	10.3	4.5	10.6 ± 0.2	21.4	Minimum horizontal stress from stable instantaneous shut-in pressures attained in final cycles.	
1218	18.8	12.1 ± 0.2	12.0	6.3	12.1 ± 0.2	25.5	Same as above.	
1288	23.8	14.8 ± 0.2	12.8	7.0	14.8 ± 0.2	27.2	Same as above.	
					USW G-2			
295	5.1	5.1 ± 0.1	2.9	0.0	5.1 ± 0.1	6.1	Reopening preexisting fracture of unknown orientation: shut-in pumping pressure is upper bound on S_h .	
418	5.4	5.4 ± 0.1	4.1	0.0	5.4 ± 0.1	8.4	Same as above.	
432	5.5	5.5 ± 0.1	4.2	0.0	5.5 ± 0.1	8.7	Same as above.	
1026	16.3	11.1 ± 0.2	10.1	4.9	11.1 ± 0.2	20.8	Minimum horizontal stress from stable pumping pressure on multiple cycles.	
1209	18.2	12.0 ± 0.2	11.8	6.7	12.0 ± 0.2	25.5	Minimum horizontal stress from flat pumping pressure attained on second cycle. S_h thus may be several bars too high due to pressure gradient in fracture.	

*Calculated for the appropriate density and depth.

†Based on water table at 576 m depth in USW G-1 and 526 m depth in USW G-2.

USW - G1

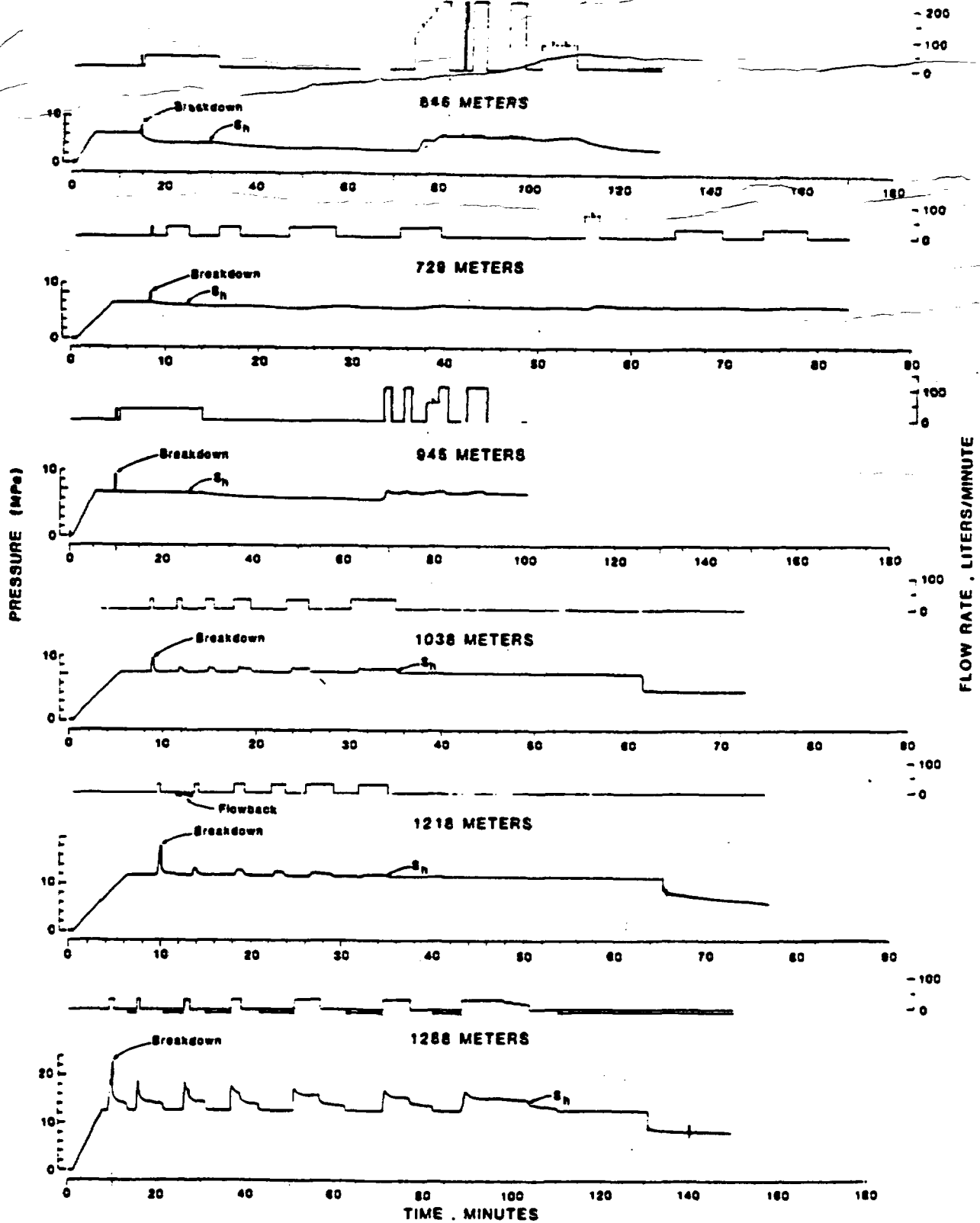


Fig. 4. Hydraulic fracturing test data from tests in USW G-1, showing downhole pressure and flow rate as a function of time.

USW G-2

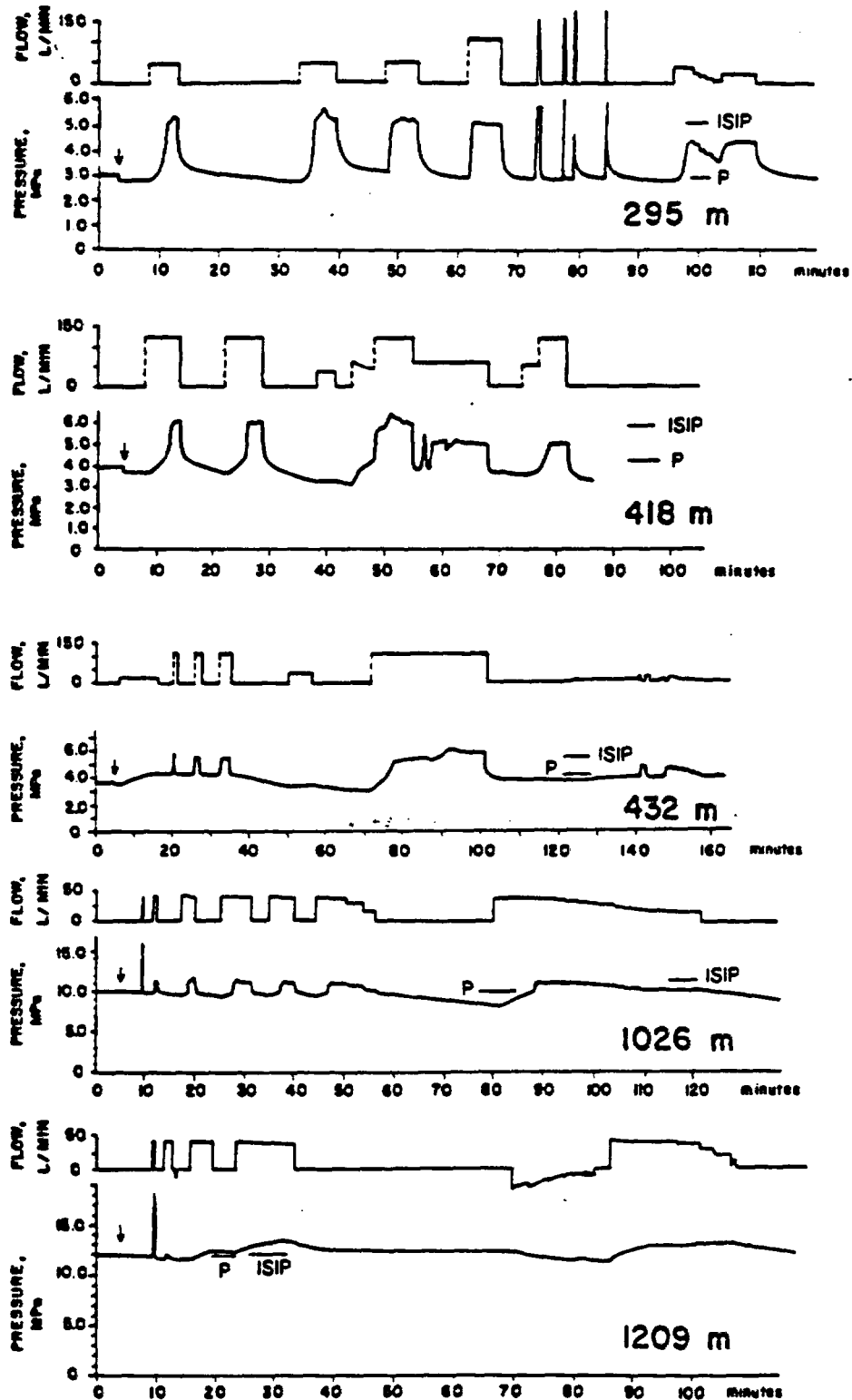


Fig. 5. Hydraulic fracturing test data from tests in USW G-2, showing downhole pressure and flow rate as a function of time. Arrows indicate time when circulation valve was opened and the interval was exposed to the pressure in the tubing string. The upper three tests were conducted above the water level in the hole, and the drop in pressure following the opening of the circulation valve results from water rushing in to replace the air in the test interval. ISIP, value of S_0 obtained from the test; P , surface hydrostatic pressure. Note the change in slope of the pressure decay curves, caused by the change in compliance of the drill pipe-packer system, when the pressure falls to the surface hydrostatic pressure P .

During this time the test interval was exposed to surface hydrostatic pressure that was 5.7 MPa above the water table hydrostatic pressure. However, because of the absence of preexisting fractures in the hydrofrac interval and the stability of the water level in the drill pipe as observed by us at the wellhead during this period, it is unlikely that this excess pressure significantly raised the pore pressure around the test interval prior to breakdown on the first cycle. After the first cycle the pressure could not be bled back to the water table hydrostatic pressure, so that the actual pore pressure during later cycles (P_p in equation (2)) may have increased through flow of water through the walls of the newly created hydraulic fracture into the formation.

For the USW G-2 tests the weighted bar and downhole pressure gauges were combined as a single wireline assembly, and a wireline lubricator was used to seal off the wellhead, so that testing could begin almost immediately after knockdown. Thus the interval was only exposed to abnormally high fluid pressures for a few minutes before breakdown. The pore pressure at the beginning of the first cycle in the USW G-2 tests can be taken as equal to the water table hydrostatic pressure without reservation. As in the USW G-1 tests, the pressure could not be bled back to the water table hydrostatic pressure after the first cycle. Therefore in both USW G-1 and USW G-2 we use the water table hydrostatic pressure as a lower bound and the ground surface hydrostatic pressure as an upper bound on the value of P_p in equation (2).

These bounding values of P_p in equation (2) were used to obtain bounding values of S_H for three of the tests: the two deepest tests in USW G-2 and the deepest test in USW G-1, all of which showed clear fracture reopening pressures significantly different from the initial breakdown pressure. Other

TABLE 2. Constraints on S_H From Hydraulic Fracturing Measurements. USW G-1 and USW G-2

	USW G-2*		USW G-1†
Depth, m	1026	1209	1288
Breakdown pressure, MPa	16.3	18.2	23.8
Shut-in pressure, MPa	11.1 ± 0.2	12.0 ± 0.2	...
Surface Hydrostatic pressure, MPa	10.1	11.8	12.8
Water Table Hydrostatic pressure, MPa	4.9	6.7	7.7
S_H , MPa	11.1 ± 0.2	12.0 ± 0.2	14.8 ± 0.2
S_H from equation (2), MPa	16.8 ± 0.4	17.3 ± 0.4	17.9
If P_p = water table hydrostat			
If P_p = surface hydrostatic pressure	11.6 ± 0.4	12.2 ± 0.4	12.8
Fracture reopening pressure, MPa	11.6	12.0	18.8
S_H , MPa	20.8	25.5	27.2

*Values of S_H derived assuming P_p = water table hydrostat are likely to be more reasonable since they imply more reasonable rock tensile strength if the resultant S_H value is used in equation (1).

†Note that since $S_1 < S_H$, P_p = surface hydrostat is too high an upper limit for P_p in equation (2).

tests were not used because they either showed fracture reopening pressures that were not significantly different from the initial breakdown pressure (shallower tests in USW G-2) or because the fracture reopening pressures were subhydrostatic and could not be accurately determined (shallower tests in USW G-1). The S_H values obtained in all three cases are greater than S_1 and less than S_3 (Table 2), so that S_H is the

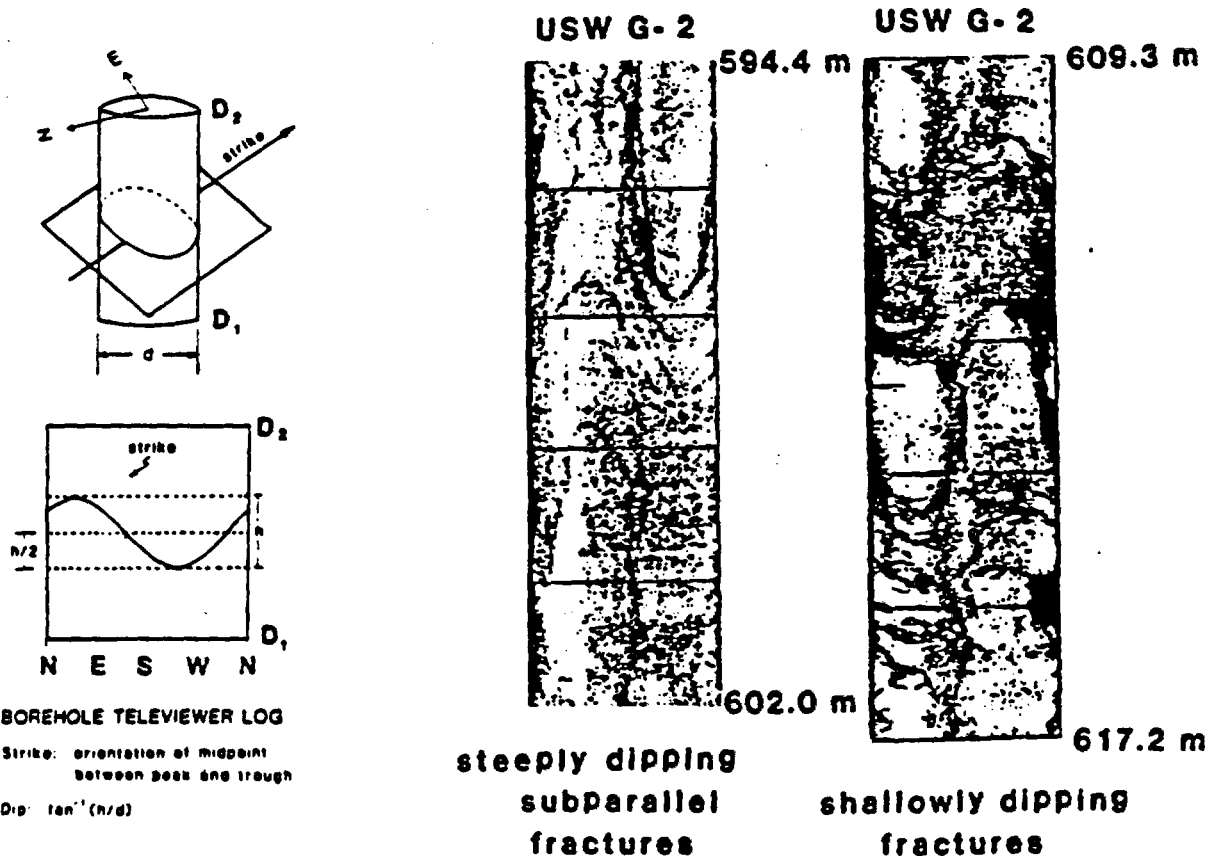


Fig. 6. Televiewer fracture with sketch of how strike and dip are measured.

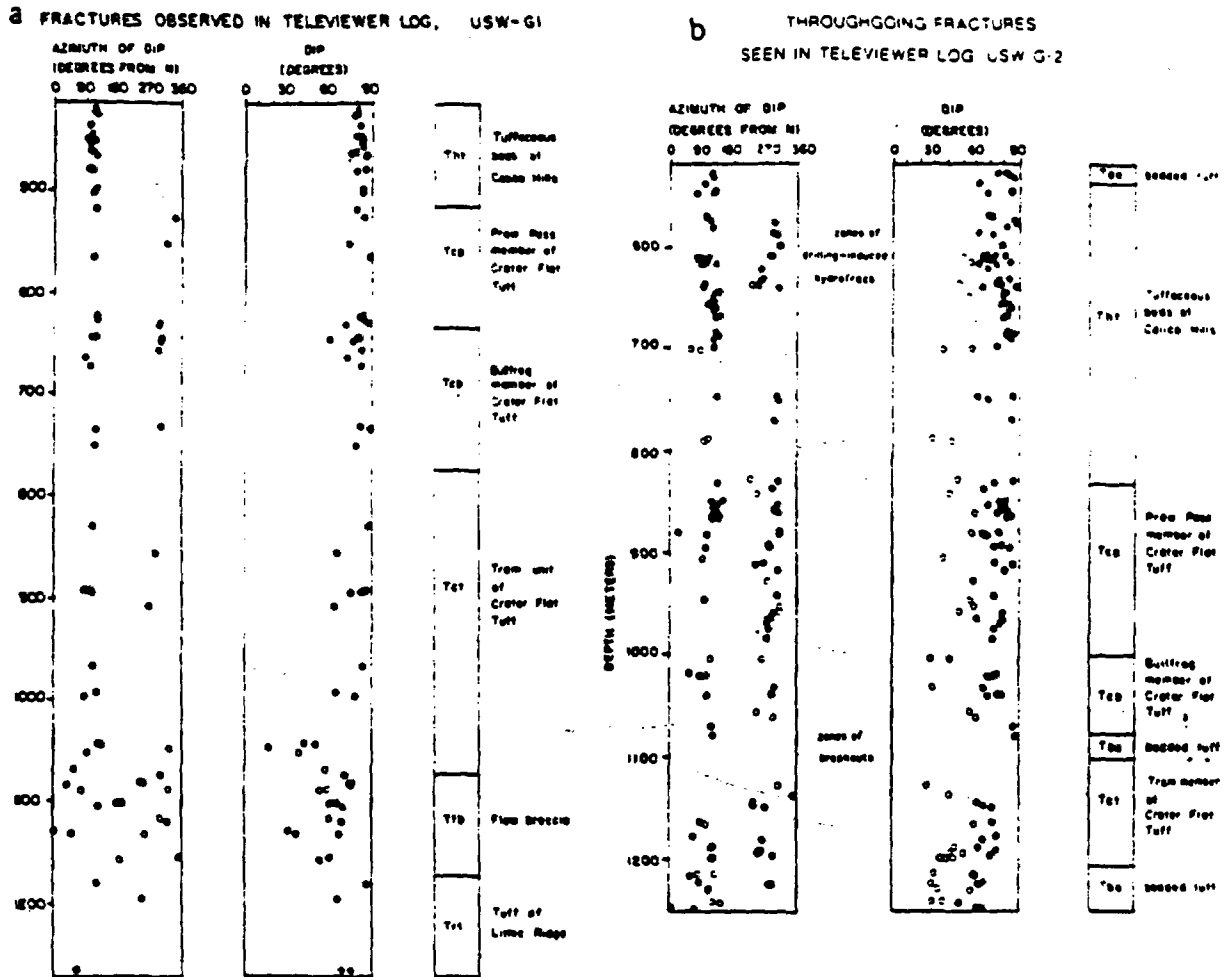


Fig. 7. Plot of azimuth and angle of dip as a function of depth for the throughgoing fractures observed in the televiewer logs of (a) USW G-1 and (b) USW G-2. The open circles represent fractures which dip less than 60°; solid circles represent fractures which dip 60° or more.

intermediate principal stress, clearly indicating a normal faulting stress regime.

Note that the use of equation (2) assuming equilibration of P_p to the surface hydrostatic pressure (our upper bound on P_p) would give S_H values very close to S_v values, implying a pure normal faulting stress regime. With S_v close to S_H in magnitude, well bore spalling would be unlikely to occur, and if it did so, it might show quite variable and discontinuous changes in orientation with depth [see Zoback et al., 1985]. The presence of continuous well bore spalling along consistent azimuths in both USW G-1 and USW G-2 implies that a considerable difference in the magnitudes of S_v and S_H is maintained at depth, so that the closer values of S_v and S_H corresponding to our upper bound on P_p are probably unlikely.

The vertical stress S_v is normally calculated as the saturated weight of the overlying rocks. Because the densities of these volcanic units vary greatly according to lithology, compaction, and degree of welding [e.g., Anderson, 1981], a constant S_v gradient could not be assumed. Values of S_v were based on integration of data from commercial borehole compensated density logs, where available, for both USW G-1 and USW G-2 (see tables of Healy et al. [1984] and Stock et al. [1984]).

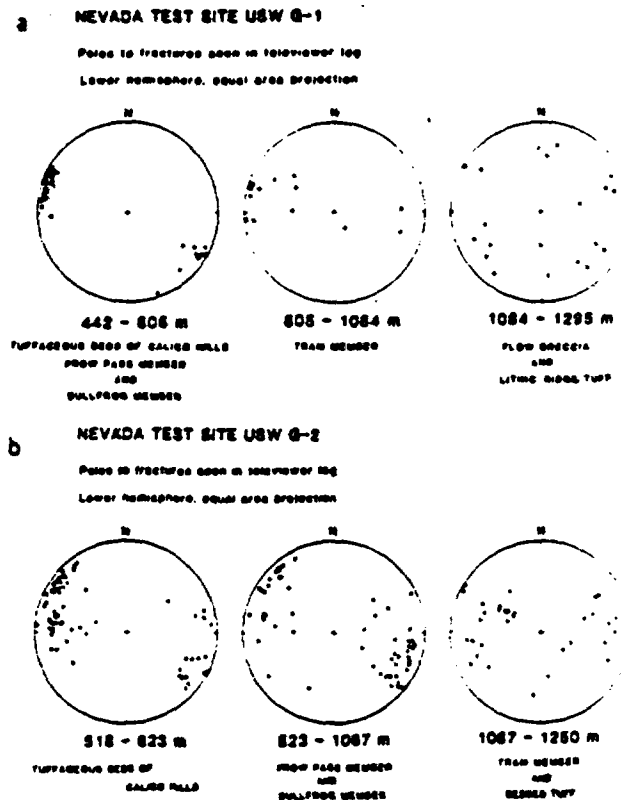


Fig. 8. (opposite) Lower hemisphere, equal-area projections of poles to the throughgoing fractures observed in the televiewer logs of (a) USW G-1 and (b) USW G-2.

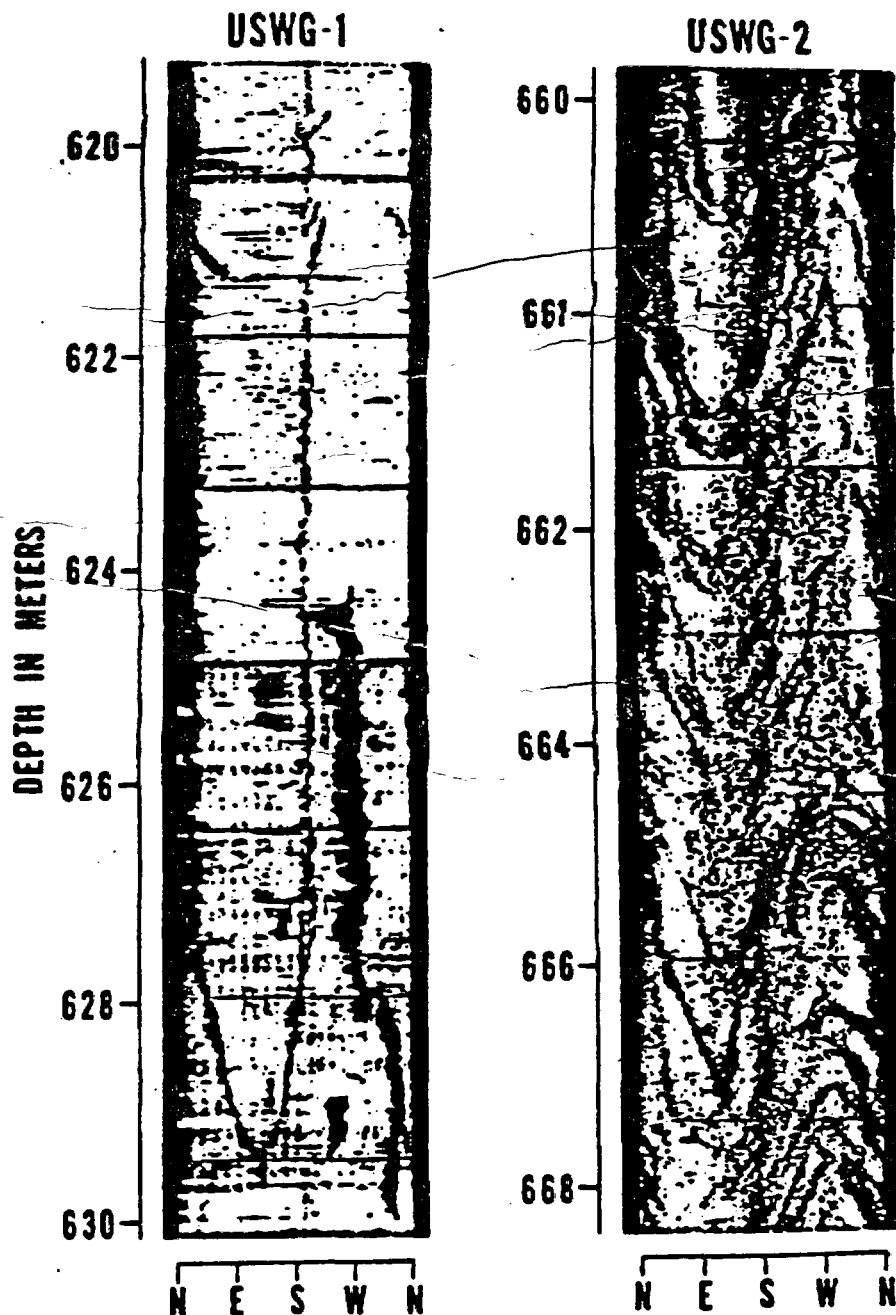


Fig. 9. Examples of drilling-induced hydrofractures, USW G-1 (10.4 cm drilled diameter) and USW G-2 (22.2 cm drilled diameter).

No borehole gravity studies were made in USW G-2, but borehole gravity measurements from USW G-1 agree very closely with the compensated density log [Snyder and Carr, 1984; D. Muller, personal communication, 1983]. This suggests that the densities obtained by compensated density logs are representative of a large region around the borehole and can be considered a reliable source for estimating S_p .

BOREHOLE TELEVIEWER

Method

The borehole televiewer is a logging tool used to map the smoothness of the borehole wall. It is useful in identifying

natural and drilling-induced fractures, borehole spalling (breakouts), and, in some cases, bedding. Principles of its operation and use have been described by Zemanek *et al.* [1969, 1970] and are briefly reviewed here.

The televiewer consists of a 2-MHz acoustic transducer which pulses 1800 times/s and rotates 3 times/s. It is pulled up the hole at a constant speed of 2.5 cm/s. The returned signal is plotted on a three-axis oscilloscope, with depth on the vertical axis, azimuth on the horizontal axis, and brightness as a function of the amplitude of the reflected pulse. A flux gate magnetometer triggers on magnetic north and emits a pulse during each revolution. Photographs of the oscilloscope display,

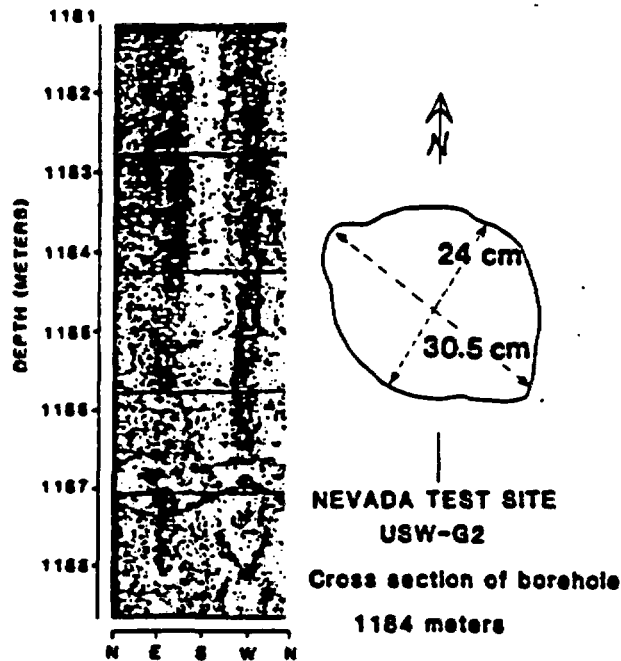


Fig. 10. Sample breakout cross section, obtained by reprocessing the returned signal from the acoustic televiewer. This part of the borehole was drilled to 22.2-cm diameter.

taken at regular intervals, are used to form a continuous log of the hole.

On the televiewer log, smooth regions of the borehole wall will appear as bright areas, and regions of roughness (e.g., fractures, breakouts) or regions that are obliquely angled with respect to the emitted pulse will show up as dark areas. For example, a planar fracture inclined to the borehole axis will appear as a sinusoidal dark band on the log. The strike and dip of such a fracture can be determined from measurement of the amplitude and phase of its trace on the televiewer photo (Figure 6). The returning signal is also recorded on magnetic tape and can be reprocessed in a travel time mode to create cross-sectional views of the hole, on which borehole spalling, tool eccentricity, and the depth of borehole wall features can be measured.

For a constant logging speed, vertical distortion of features in the log varies with borehole diameter. Since USW G-1 was about half the size of USW G-2 (10.4-cm bit diameter versus 22.2-cm bit diameter), there is greater horizontal exaggeration on the USW G-1 log. This exaggeration improves the resolution of steeply dipping features but makes the identification of shallowly dipping features more difficult. In general, for the logging speed used, resolution is limited to features dipping more than 30°.

Results

Televiewer logs were obtained in USW G-1 from 1318 to 450 m and in USW G-2 from 1250 to 526 m. Both holes were blocked at the bottom of the logged interval; the top of the logged interval is the fluid level in the hole. The complete logs, obtained prior to hydraulic fracturing, have been reproduced by Healy et al. [1984] and Stock et al. [1984]. Logs were run after testing to check for changes in the test intervals and for hydraulic fractures, but no differences between these logs and the earlier logs were observed. Although the entire logs are too long to be presented here, some of the more interesting features are discussed.

Throughgoing fractures (defined as fractures for which both updip and downdip intersections with the hole are visible on the televiewer log) are present at all depths. The majority of these dip at angles greater than 60°. Plots of the dip direction as a function of depth for fractures in USW G-1 (Figure 7a) show that in the upper part of USW G-1, these fractures strike slightly east of north and usually dip steeply to the ESE. Below about 1050 m they have more scattered orientations, and some quite shallow dips are observed. Many more fractures are seen in the USW G-2 televiewer log (Figure 7b) than in the USW G-1 log. In the upper 500 m of the USW G-2 log the fractures show a preferred orientation of NNE strikes and high-angle dips (greater than 60°) to either ESE or WNW. A few fractures with dips less than 60° occur throughout the log. The scatter in dip direction increases slightly with depth for both low-angle and high-angle fractures.

Stereographic projections of poles to the throughgoing fractures (Figure 8) show that in USW G-2 the fractures clearly become less steep with depth. This is also the case for the fractures seen in USW G-1, although it is a much more abrupt change.

Most of these fractures cannot be easily correlated with fractures in the core because the core was not oriented with respect to north. Although larger fault zones seen in the televiewer logs can be correlated with similar features in the core, there are many more fractures in the core than in the televiewer log. Some of these may be due to the coring process; many are probably preexisting fractures that were too small to be resolved by the televiewer. We infer that most of the throughgoing fractures seen in the televiewer log were present before drilling; the NW to NE strikes are consistent with surface observations of NW to NE trending faults on Yucca Mountain (Figure 2).

Very high angle, nonthroughgoing fractures are also prominent in the upper part of the televiewer logs (Figure 9). In USW G-1 these occur between 520 and 760 m depth, as long single fractures with strikes between N15°E and N35°E. In USW G-2 they occur between 526 and 678 m depth, as an echelon subparallel fractures merging into one another along a strike of N25°E to N30°E. Because some of the corresponding sections of core are unfractured, these fractures were probably created after coring. We believe that these are hydrofractures induced by the drilling process, which are oriented perpendicularly to the S_1 direction (implying that $S_1 = N65°W$ in USW G-1 and $N60°W$ in USW G-2). The stress conditions required to form these fractures are discussed later.

Throughout large sections of the USW G-1 televiewer log and at depth in the USW G-2 televiewer log, vertical black bands occur in pairs centered at azimuths approximately 180° apart. There are two types of black bands: very regular, continuous black bands with fuzzy, gradational edges and more irregular bands, often discontinuous, with sharp, jagged edges. These were examined by reprocessing the recorded signal in travel time mode to produce a horizontal cross section of the hole [see Zoback et al., 1985]. The travel time cross sections of these bands demonstrate that the regular, continuous bands are due to the tool being off center in the hole. These dark bands are more prominent in the USW G-1 televiewer log because USW G-1 had a drift of up to 12° toward the southwest (Figure 3). USW G-2 had a maximum drift less than 5°, so the tool was usually well centered and these regular black bands were not observed.

By contrast, the jagged, irregular black bands were found to correspond to preferentially enlarged (spalled) regions of the

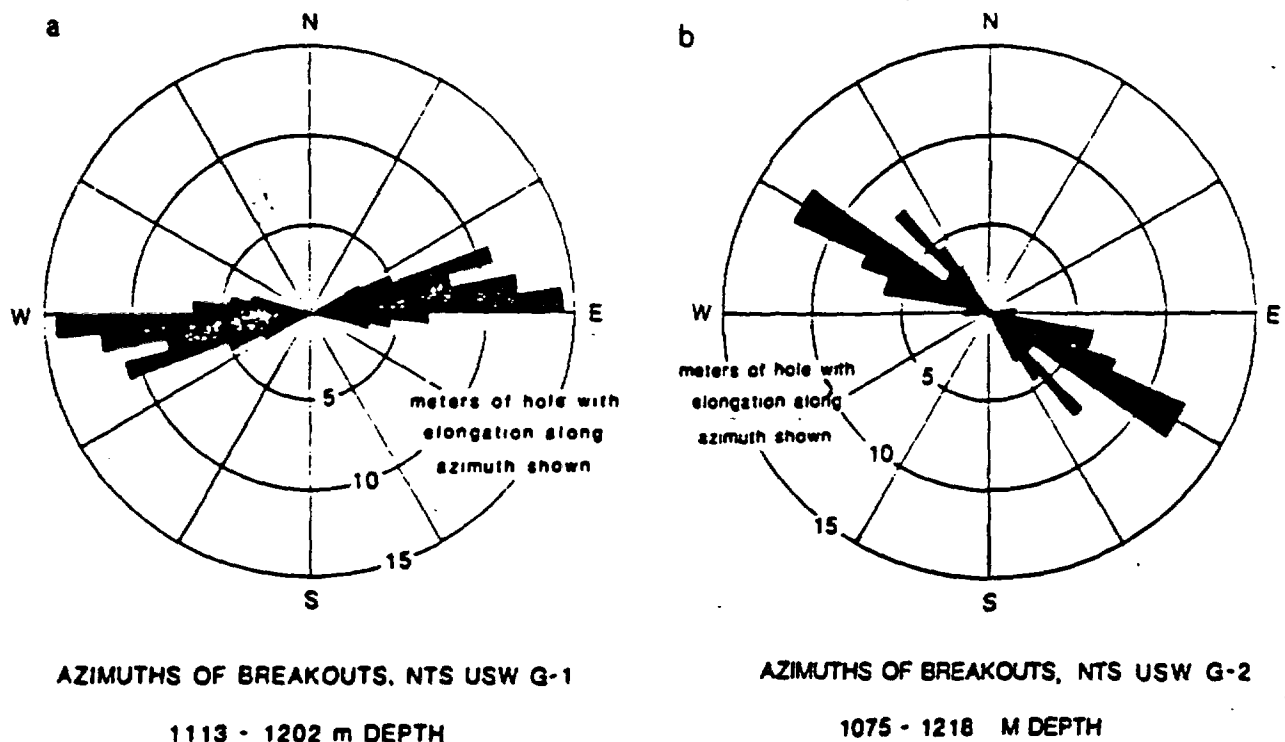


Fig. 11. Rose diagrams of the observed orientations of breakouts, averaged (a) over each 0.3-m interval in USW G-1 and (b) over each 1.5-m interval in USW G-2.

borehole (Figure 10). Their cross-sectional shapes varied from pointed or triangular to elliptical. Such regions of preferential spalling, or borehole breakouts, have also been identified on dipmeter logs from wells in Alberta, the Texas Gulf Coast, and Colorado [e.g., Bell and Gough, 1983]. Breakouts are believed to represent shear failure of the borehole wall in the region of high concentrated compressive stresses, centered on the azimuth of S_1 [Bell and Gough, 1979; Gough and Bell, 1981, 1982; Zoback et al., 1985]. Comparison of the direction of borehole elongation obtained from a borehole televiewer log with the azimuth of S_1 determined from hydraulic fracturing tests in the same well in central New York state [Hickman et al., 1985] as well as the agreement between the azimuth of S_1 as inferred from breakouts and that inferred from other field indicators within a given stress province [Zoback and Zoback, 1980; R. Plumb, manuscript in preparation, 1985] confirm this hypothesis. In addition, laboratory studies of breakout development by Mastin [1984] indicate that breakouts do occur centered at the azimuth of S_1 due to a combination of shear and tensile failure of the borehole wall.

In USW G-1, breakouts were continuously present from 1113 to 1202 m depth, with an average azimuth of $S_80^\circ W$ (Figure 11a). In USW G-2, breakouts were present at depths of 1053–1056, 1074, and 1084–1219 m, with an average azimuth of $N60^\circ W$ (Figure 11b). The center azimuths of the breakouts thus suggest a $N60^\circ$ – $65^\circ W$ orientation for S_1 in USW G-2, in good agreement with the S_1 direction indicated by the orientation of the drilling-induced hydrofractures in the upper parts of both USW G-1 and USW G-2. This direction is also in good agreement with that obtained from observations of borehole breakouts and drilling-induced hydraulic fractures in two other holes at Yucca Mountain, in the volcanics and underlying carbonate rocks [Stock and Healy, 1984]. The center azimuth of the USW G-1 breakouts implies an S_1 direction of $S80^\circ W$, a 35° – 40° difference from the other directional

indicators. Although deviation of the borehole from the vertical has been shown to have a significant effect on the orientation of stress-induced features such as hydraulic fractures [Richardson, 1983], calculations using the observed Yucca Mountain stress field ($S_1 =$ vertical, $S_2 = N25^\circ E$, $S_3 = N65^\circ W$, and $0.25 \leq (S_2 - S_3)/(S_1 - S_2) \leq 0.5$) show that the hole deviation at this depth cannot completely account for the rotation of breakout azimuths. Deviation can explain this rotation if the greatest principal stress direction is more than 10° from vertical, or if S_1 and S_2 are closer in magnitude than seen elsewhere at Yucca Mountain (Table 2 and Stock and Healy [1984]). Because the anomalously oriented breakouts occur in a fractured zone of flow breccia, such a local perturbation in the magnitude and/or direction of the principal stresses seems a likely possibility.

DISCUSSION OF STRESS MEASUREMENTS

Stability of Preexisting Faults

A preexisting fault will slip if the shear stress τ applied to the fault surface reaches a value equal to $(s_n - P_n) \mu$ (the effective normal stress multiplied by the coefficient of friction, μ). Under the stresses observed in the saturated zone of Yucca Mountain ($S_1 > S_2 > S_3$ with S_1 oriented $N65^\circ W$) the plane with the highest ratio of shear to effective normal stress (the most favorable plane for slip) would strike parallel to S_2 ($N25^\circ E$) and dip either east or west at an angle θ related to the coefficient of friction μ by $2\theta = (\tan^{-1} \mu + 90^\circ)$. For typical values of μ (between 0.6 and 1.0 [Byerlee, 1978]), such planes dip between 60° and 67° . There are mapped faults at Yucca Mountain of approximately this orientation (Figure 2 and Scott and Bank [1984]), and fractures of this orientation are also seen in the televiewer logs, as discussed above. Laboratory compressive strength tests of the Yucca Mountain tuffs (summarized by Price [1983]) indicate that in the ob-

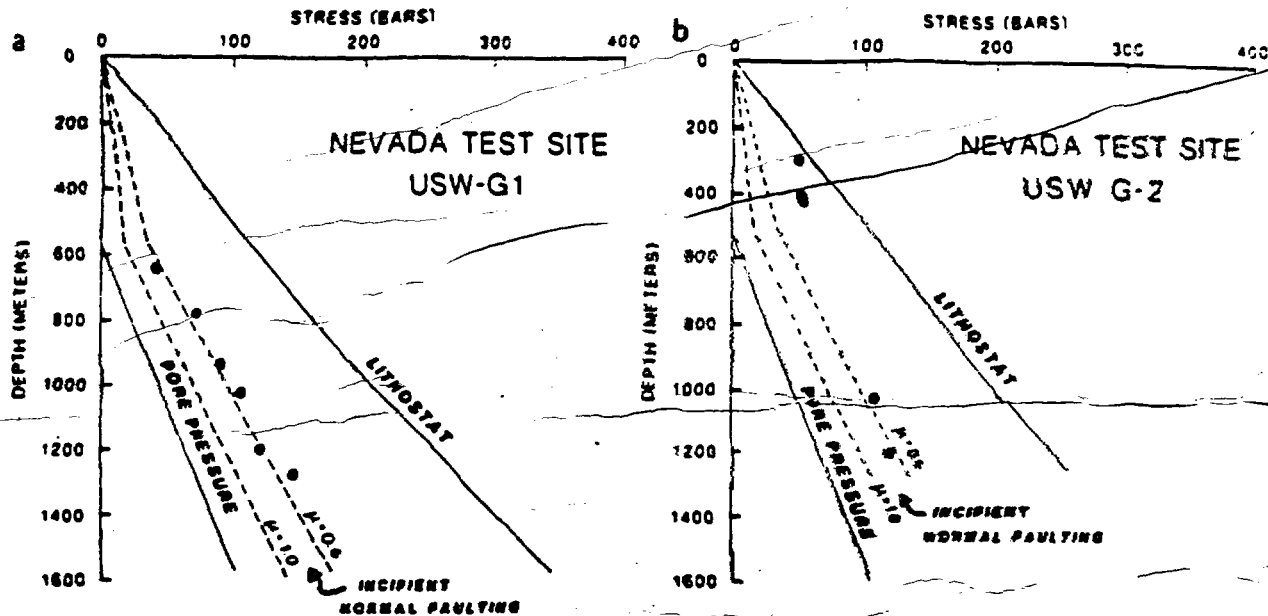


Fig. 12. Least horizontal principal stress values for (a) USW G-1 and (b) USW G-2 plotted against depth. Lithostatic pressure S_L and pore pressure (based on depth to water level in hole) are also shown. Stress values falling to the left of the dashed lines correspond to those for which slip might be expected to occur on preexisting favorably oriented normal faults, for reasonable values of the coefficient of friction, μ (0.6 to 1.0). Note that the upper three measurements in USW G-2 are upper limits on the value of S_2 (see text for discussion).

served stress regime, slip would occur preferentially on these faults rather than through the shear failure of intact rock.

For a favorably oriented fault plane, the expression $\tau = \mu(s_1 - P_p)$ can be rewritten in terms of the principal stresses as

$$\frac{S_1 - P_p}{S_3 - P_p} = [\mu + (\mu^2 + 1)^{1/2}]^2$$

[e.g., McGarr et al., 1982; Zoback and Hickman, 1982; Zoback and Healy, 1984]. In a normal faulting environment, such as the saturated zone of Yucca Mountain, $S_1 = S_L$ and $S_3 = S_p$; S_1 and P_p are well constrained as a function of depth. Therefore, if μ is known, the condition for slip on a favorably oriented fault at a given depth can be defined in terms of a critical value of S_3 . If S_3 exceeds this value, no slip will take place on any faults, but if S_3 is equal to or less than this value, slip will occur on favorably oriented preexisting faults.

Byerlee [1978] demonstrated that almost all rocks have laboratory coefficients of friction between 0.6 and 1.0. We therefore use these two bounding values of μ to compute critical values for S_3 as a function of depth for our measurements in the saturated zone (Figure 12). Measured S_3 values are close to those for which slip might take place on favorably oriented preexisting faults, if $\mu = 0.6$. Slip should not occur if $\mu = 1.0$. Laboratory coefficients of friction for samples of the Topopah Springs and Bullfrog member range from 0.7 to 0.9 [Morrow and Byerlee, 1984]. A value of 0.59 has been reported for the Prow Pass member [Olsson and Jones, 1980]. These values suggest that in at least part of the tuff section at Yucca Mountain, favorably oriented preexisting faults might slip under the current stress conditions.

Formation of Drilling-Induced Hydrofractures

Preexisting cracks of fairly large size are likely to have been present in USW G-1 and USW G-2, since much of the core contains lithophysal cavities, pumice fragments, lithics, and phenocrysts exceeding 1 cm in size. It therefore seems quite

plausible that propagation of preexisting flaws occurred during drilling, as the hole was filled with fluid and downhole pumping pressure was applied. Such fractures would continue to propagate away from the borehole if the fluid pressure in them exceeded S_3 . Pressures during drilling may have easily exceeded S_3 throughout much of USW G-1 and possibly also USW G-2 (Figure 13). We believe that this is the origin of the long, planar fractures which are prominent in both the USW G-1 and USW G-2 televiwer logs (as described above in televiwer results). The complete loss of circulation fluid experienced during drilling of these two holes can be explained by the fluid going into the drilling-induced fractures.

RELATIONSHIP OF YUCCA MOUNTAIN STRESSES TO THE REGIONAL STRESS FIELD

The Nevada Test Site falls at the eastern edge of the stress transition zone defined by Zoback and Zoback [1980] between WNW-ESE extension characteristic of the Basin and Range province and the strike-slip faulting characteristic of the San Andreas stress province. Because both normal and strike-slip faulting occur at NTS, the magnitudes of the principal stresses have been inferred to be at the transition between normal and strike-slip stress regimes ($S_2 = S_H > S_3$). The few published regional focal mechanisms from events at depths from 0.8 to 10.2 km have almost exclusively strike-slip solutions (Figure 14).

The NW to WNW extension direction indicated by the regional data (Table 3) agrees very well with the S_1 direction of N60°W to N65°W seen in the Yucca Mountain drill holes. The magnitudes of S_1 measured by the hydraulic fracturing technique are also close to the value of $S_1 = 1/2S_L$ determined by McGarr [1982] to be characteristic of the transition zone. However, at the depths of our measurements, Yucca Mountain is within a normal faulting stress regime, with S_H about halfway between S_2 and S_3 in magnitude. This is significantly different from the stress regime with $S_H = S_2$ that has usually

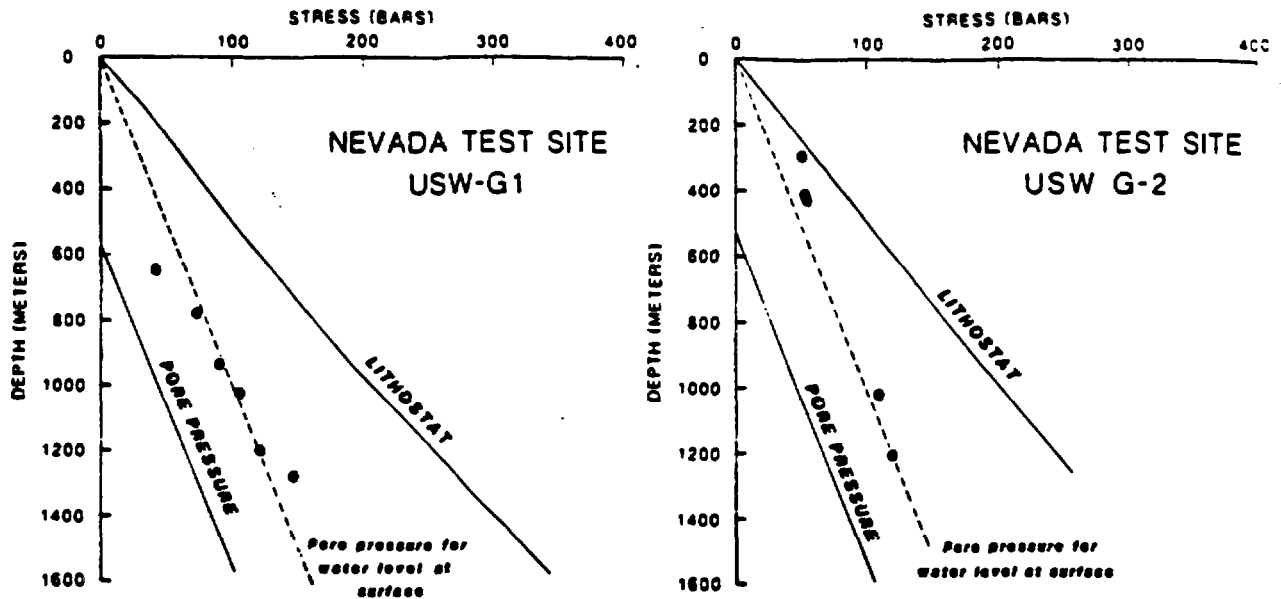


Fig. 13. Measured values of the least horizontal principal stress S_3 as a function of depth in USW G-1 and USW G-2. Pore pressure line corresponding to the observed water level in each hole is shown for reference. The dashed line is the pore pressure curve which would be expected if the hole were filled to the surface with water. The measured values of S_3 suggest that the fluid pressure in the hole may have exceeded S_3 during drilling, causing drilling-induced hydraulic fractures to form and propagate. Note that the upper three measurements in USW G-2 are upper limits on the value of S_3 (see text for discussion).

TABLE 3. Compilation of Stress Indicators, NTS Area

No.	Location	Type of Measurement	S_3 Direction	Stress Regime	Age of Indicator	Reference	Comments
1	Rainier Mesa	hydrofrac	N55°W	strike slip (ss)	0	Haimson et al. [1974]	all of these measurements may be strongly influenced by topography
2	Rainier Mesa	hydrofrac (in center of mesa)	NW-SE	normal/ss	0	Smith et al. [1981]	
3	Rainier Mesa and Aqueduct Mesa	overcooring	NW-SE to E-W	mainly ss some normal	0	Ellis and Magner [1980]	all of the measurements may be strongly influenced by topography
4	Pahute Mesa	explosion produced fractures in tuff	WNW-ESE to E-W	normal	0	Snyder [1971]	
5	Pahute Mesa	borehole breakouts	N50°W	?	0	Springer and Thorpe [1981]	
6	Yucca Flat	explosion produced fractures in alluvium	N50°W	normal	0	Carr [1974]	fractures in alluvium likely to be affected by basin structure
7	Yucca Flat	borehole breakouts	N60°W	?	0	Carr [1974]	
8	Yucca Flat	borehole breakouts	N45°W	?	0	Springer and Thorpe [1981]	
9	Crater Flat (east)	trenching of Quaternary faults	N70°-80°W	?	0.1 m.y.	Swadley and Hoover [1984]	exact displacement direction unknown
10	Crater Flat	alignment of cinder cones	N60°W ± 10°	normal	1.1 m.y.		indicators are too old and their orientation may be related to pre-existing fractures
11	Crater Flat	dikes	E-W to WNW	normal	3.75 m.y.		indicators are too old and their orientation may be related to pre-existing fractures
12	NTS area	focal mechanism P axes	NW to W	ss/normal	0	Rogers et al. [1983]	uncertainty in relationship between P axes and S_3 direction
13	Pahute Mesa	focal mechanism P axes	NW to W	ss/normal	0	Hamilton and Healy [1969]	uncertainty in relationship between P axes and S_3 direction
14	Yucca Mountain	drilling-induced hydraulic fractures	N60°-N70°W	normal	0	this report	

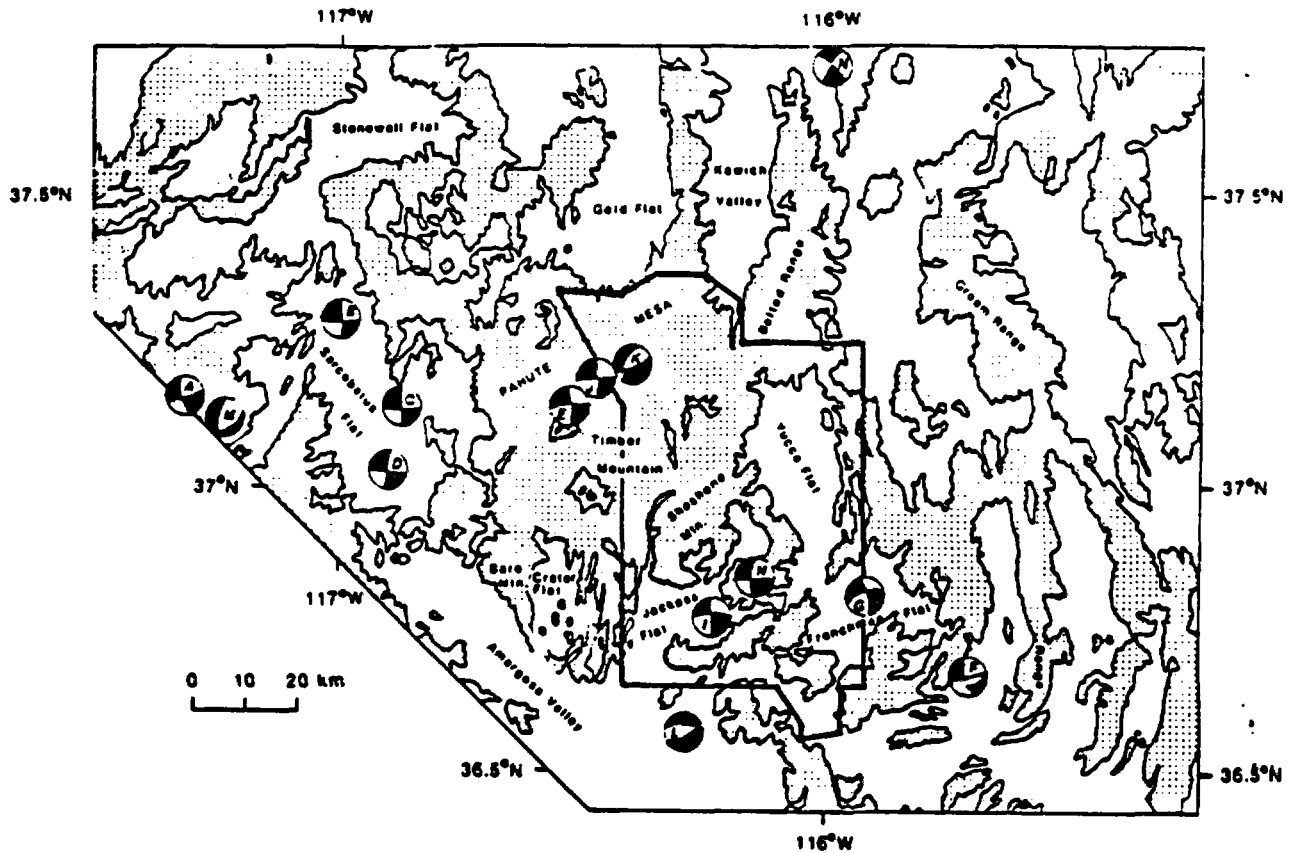


Fig. 14. Compilation of NTS region focal mechanisms. Letters correspond to event identification from Table 4.

been assumed for the area. Yucca Mountain could be locally anomalous, having a much lower relative magnitude of S_H than most of the surrounding region. However, no change in stress regime is actually required by the presence of strike-slip faulting in the area.

The reported focal mechanisms do not have a uniform distribution of nodal plane orientations. The nodal planes are nearly all steeply dipping, with N to NE strike, and show strike-slip faulting, with minor normal component [Rogers et al., 1983]. Resolution of the Yucca Mountain stress tensor

TABLE 4. Focal Mechanisms Compiled for the NTS Region

Event	Date	Depth, km	Location	Reference
A	Jan. 23, 1981	10.2	37.148°N, 117.387°W Gold Mountain	Rogers et al. [1983]
B	Dec. 25, 1979	8.1	37.288°N, 114.062°W Sarcobatus Flat	Rogers et al. [1983]
C	March 10, 1981	6.6	37.155°N, 116.917°W Sarcobatus Flat	Rogers et al. [1983]
D*	Aug. 17, 1979	9.2	37.055°N, 116.955°W Sarcobatus Flat	Rogers et al. [1983]
E*	Aug. 17, 1979	6.3	37.185°N, 116.570°W Thirsty Canyon	Rogers et al. [1983]
F*	Dec. 26, 1981	8.6	36.725°N, 115.708°W Indian Springs	Rogers et al. [1983]
G	April 2, 1980	1.4	36.860°N, 115.961°W Frenchman Flat	Rogers et al. [1983]
H	April 23, 1980	6.7	36.874°N, 116.162°W Lookout Peak	Rogers et al. [1983]
I	May 10, 1980	0.8	36.811°N, 116.267°W Jackass Flats	Rogers et al. [1983]
J*	Dec. 1968		Aftershocks of Benham explosion	Hamilton and Healy [1969]
K*	Dec. 1968		Aftershocks of Benham explosion	Hamilton and Healy [1969]
L	Feb. 12, 1970		36.60°N, 116.27°W	Smith and Lindh [1978]
M	Sept. 1970		37.13°N, 117.32°W	Smith and Lindh [1978]
N	March 23, 1970		37.75°N, 116.00°W	Smith and Lindh [1978]

*Composite mechanism.

($S_1 > S_2 > S_3$, with S_2 oriented N65°W and S_3 about halfway between S_1 and S_2 in magnitude) onto planes of the reported orientations indicates that the direction of maximum shear (expected direction of slip vector) on these planes would be close to horizontal, and could be parallel to the observed slip vectors (J. M. Stock, manuscript in preparation, 1985). Thus, if these nodal planes were preexisting faults, subjected to the Yucca Mountain stress regime, they could produce strike-slip focal mechanisms consistent with those observed.

Yucca Mountain itself has very few observed earthquakes, compared to surrounding areas of NTS [Rogers et al., 1983]. Although there are faults of known Quaternary displacement in the area, results of trenching, as of this publication date, indicate no conclusive evidence of Holocene offset [Swadley et al., 1984]. Given the available laboratory measurements showing values of μ of 0.6 to 0.9 [Morrow and Byerlee, 1984], the measured stresses at Yucca Mountain are near the limit of those required to cause slip on favorably oriented preexisting faults. Scatter in both the laboratory and the field data cannot preclude the possibility that stress values might reach the levels required to cause seismic or aseismic motion on the faults.

Brace and Kohlstedt [1980] showed that Byerlee's law describing the frictional behavior of rocks [Byerlee, 1978] correctly gives the limiting value of lithospheric stresses in all cases of measured in situ stresses to depths of at least 4 km. In areas of active normal faulting, the magnitude of the least horizontal stress relative to the vertical stress can be shown to be controlled by the vertical stress and frictional stability of preexisting faults, at the limit expected from Byerlee's law [Zoback and Healy, 1984]. In such areas the minimum principal stress values measured from hydrofrac tests are very close to the values at which slip would occur on favorably oriented faults. The measurements at Yucca Mountain fit this pattern. Since active faulting is occurring throughout the NTS area, as shown by recent seismicity and Quaternary offsets, it is expected that S_2 and S_3 should follow the values of frictional stability expected from Byerlee's law. Therefore the direction of S_2 and the relative magnitudes of S_2 and S_3 measured at Yucca Mountain are probably typical of the general regional stress pattern.

CONCLUSIONS

Hydraulic fracturing stress measurements in holes USW G-1 and USW G-2 at Yucca Mountain show that both the least and greatest horizontal principal stresses (S_2 and S_3 , respectively) are less than the vertical stress S_1 . The measured stresses correspond to a normal faulting regime with S_3 about halfway between S_2 and S_1 . The observed magnitudes of S_2 and S_3 indicate that frictional sliding might be expected to occur on favorably oriented preexisting faults if the coefficient of friction along such faults were close to 0.6. For coefficients of friction close to 1.0, all preexisting faults should be stable. Laboratory tests of the Yucca Mountain volcanic rocks yield coefficients of friction ranging from 0.6 to 0.9, suggesting that some favorably oriented preexisting fault zones might experience frictional sliding under the measured stress conditions. Seismic and geological observations, however, argue otherwise.

Borehole televiwer observations of USW G-1 and USW G-2 reveal that the S_2 direction is N65°W \pm 10°, as determined by (1) the N25°E to N30°E strike of long, drilling-induced hydraulic fractures seen to 760 m depth in USW G-1 and 680 m depth in USW G-2 and (2) the average N65°W

orientation of borehole breakouts seen from 1050 to 1220 m in the USW G-2 televiwer log. Breakouts in USW G-1, seen from 1113 to 1202 m, have an average orientation of S80°W and are believed to be affected by a local perturbation in stress direction in this zone (consisting of highly fractured flow breccia which is not present in USW G-2). Owing to limitations on drill rig time, no orientations of test-induced hydrofractures were obtained.

These measurements are in good agreement with other stress indicators from the Nevada Test Site which yield a NW-SE to WNW-ESE direction of S_2 . Although both normal and strike-slip faulting patterns are observed at NTS, calculations of slip on preexisting faults show that the observed strike-slip focal mechanisms could occur in response to a normal faulting stress regime similar to that measured at Yucca Mountain.

Acknowledgments. We thank J. Svittek, D. Styles, J. Hennagan, and G. Zwart for invaluable help in the operation and maintenance of field equipment and Larry Mastin for discussions of breakout theory and observations. This work would not have been possible without the generous advice and assistance of Ray Escobedo, Wallace Hamner, and other personnel of Fenix and Scisson, Inc. Thoughtful reviews by A. McGarr, P. Segall, and W. F. Brace are greatly appreciated. J. M. Stock was partially supported by the Fannie and John Hertz Foundation. The work was performed in cooperation with the Nevada Operations Office of the U.S. Department of Energy under interagency agreement DE-AJ08-78ET44802.

REFERENCES

- Anderson, L. A., Rock property analysis of core samples from the Yucca Mt. UE25a #1 borehole, Nevada Test Site, Nevada, U.S. Geol. Surv. Open File Rep., 81-1338, 1981.
- Bell, J. S., and D. I. Gough, Northeast-southwest compressive stress in Alberta: Evidence from oil wells, *Earth Planet. Sci. Lett.*, 45, 475-482, 1979.
- Bell, J. S., and D. I. Gough, The use of borehole breakouts in the study of crustal stress, in *Hydraulic Fracturing Stress Measurements*, edited by M. D. Zoback and B. C. Haimson, pp. 201-209, National Academy Press, Washington, D. C., 1983.
- Brace, W. F., and D. L. Kohlstedt, Limits on lithospheric stress imposed by laboratory experiments, *J. Geophys. Res.*, 85, 6248-6252, 1980.
- Bredehoeft, J. D., and S. S. Papadopoulos, A method for determining the hydraulic properties of tight formations, *Water Resour. Res.*, 16, 233-238, 1980.
- Bredehoeft, J. D., R. G. Wolff, W. S. Keys, and E. Shuter, Hydraulic fracturing to determine the regional in-situ stress field, Piceance Basin, Colorado, *Geol. Soc. Am. Bull.*, 87, 250-258, 1976.
- Byerlee, J. D., Friction of rocks, *Pure Appl. Geophys.*, 116, 615-626, 1978.
- Carr, W. J., Summary of tectonic and structural evidence for stress orientation at the Nevada Test Site, U.S. Geol. Surv. Open File Rep., 74-176, 1974.
- Carr, W. J., Volcano-tectonic history of Crater Flat, southwestern Nevada, as suggested by new evidence from drill hole USW VH-1 and vicinity, U.S. Geol. Surv. Open File Rep., 82-457, 1982.
- Cooper, H. H., J. D. Bredehoeft, and I. S. Papadopoulos, Response of a finite-diameter well to an instantaneous charge of water, *Water Resour. Res.*, 3, 263-269, 1967.
- Earlougher, R. C., *Advances in Well Test Analysis*, AIME Monogr., vol. 5, American Institute of Mining, Metallurgical, and Petroleum Engineers, Dallas, Tex., 1977.
- Ellis, W. L., and J. E. Magner, Compilation of results of three-dimensional stress determinations made in Rainier and Aqueduct mesas, Nevada, U.S. Geol. Surv. Open File Rep., 80-1098, 1980.
- Gough, D. I., and J. S. Bell, Stress orientations from oil-well fractures in Alberta and Texas, *Can. J. Earth Sci.*, 18, 638-645, 1981.
- Gough, D. I., and J. S. Bell, Stress orientation from borehole wall fractures with examples from Colorado, east Texas, and northern Canada, *Can. J. Earth Sci.*, 19, 1358-1370, 1982.
- Haimson, B. C., and J. M. Avasthi, Stress measurements in anisotropic rock by hydraulic fracturing, *Proc. U. S. Symp. Rock Mech.*, 15th, 135-156, 1975.

- Haimson, B. C., and C. Fairhurst, Initiation and extension of hydraulic fractures in rock. *Soc. Pet. Eng. J.*, 7, 310-318, 1967.
- Haimson, B. C., and C. Fairhurst, In-situ stress determinations at great depths by means of hydraulic fracturing. *Proc. U.S. Symp. Rock Mech.*, 11th, 559-584, 1970.
- Haimson, B. C., J. Lacombe, A. H. Jones, and S. J. Green, Deep stress measurement in tuff at the Nevada Test Site, in *Advances in Rock Mechanics*, vol. IIa, pp. 557-561, National Academy of Sciences, Washington, D. C., 1974.
- Hamilton, R. M., and J. H. Healy, Aftershocks of the Benham nuclear explosion. *Bull. Seismol. Soc. Am.*, 59, 2271-2281, 1969.
- Healy, J. H., S. H. Hickman, M. D. Zoback, and W. L. Ellis, Report on televiewer log and stress measurements in core hole USW-G1, Nevada Test Site, *U.S. Geol. Surv. Open File Rep.*, 84-15, 1984.
- Hickman, S. H., and M. D. Zoback, The interpretation of hydraulic fracturing pressure-time data for in-situ stress determination, in *Hydraulic Fracturing Stress Measurements*, edited by M. D. Zoback and B. C. Haimson, pp. 44-54, National Academy Press, Washington, D. C., 1983.
- Hickman, S. H., J. H. Healy, and M. D. Zoback, In situ stress, natural fracture distribution, and borehole elongation in the Auburn geothermal well, Auburn, New York, *J. Geophys. Res.*, 90, 5497-5512, 1985.
- Hoffman, L. R., and W. D. Mooney, A seismic study of Yucca Mountain and vicinity, southern Nevada: Data report and preliminary results, *U.S. Geol. Surv. Open File Rep.*, 83-388, 1983.
- Hubbert, M. K., and D. G. Willis, Mechanics of hydraulic fracturing. *J. Pet. Technol.*, 9, 153-168, 1957.
- Hudson, J. A., A critical examination of indirect tensile strength tests for brittle rocks. Ph.D. thesis, Univ. of Minnesota at Minneapolis St. Paul, Minneapolis, 1971.
- Maldonado, F., and S. L. Koether, Stratigraphy, structure, and some petrographic features of Tertiary volcanic rocks at the USW G-2 drill hole, Yucca Mountain, Nye County, Nevada, *U.S. Geol. Surv. Open File Rep.*, 83-732, 1983.
- Marvin, R. F., F. M. Byers, Jr., H. H. Mehnert, P. P. Orkild, and M. W. Stern, Radiometric ages and stratigraphic sequence of volcanic and plutonic rocks, southern Nye and western Lincoln counties, Nevada. *Geol. Soc. Am. Bull.*, 81, 2657-2676, 1970.
- Martin, L. G., Development of borehole breakouts in sandstone, M.S. thesis, Stanford Univ., Stanford, Calif., 1984.
- McGarr, A., Analysis of states of stress between provinces of constant stress. *J. Geophys. Res.*, 87, 9279-9288, 1982.
- McGarr, A., M. D. Zoback, and T. C. Hanks, Implications of an elastic analysis of in situ stress measurements near the San Andreas fault. *J. Geophys. Res.*, 87, 7797-7806, 1982.
- Morrow, C., and J. Byerlee, Frictional sliding and fracture behavior of some Nevada Test Site tuffs, *Proc. U.S. Symp. Rock Mech.*, 25th, 467-474, 1984.
- Olsson, W. A., and A. K. Jones, Rock mechanics properties of volcanic tuffs from the Nevada Test Site, *Rep. SAND80-1453*, Sandia Natl. Lab., Albuquerque, N. M., 1980.
- Price, R. H., Analysis of rock mechanics properties of volcanic tuff units from Yucca Mountain, Nevada Test Site, *Rep. SAND82-1315*, Sandia Natl. Lab., Albuquerque, N. M., 1983.
- Ratigan, J. L., A statistical fracture mechanics determination of the apparent tensile strength in hydraulic fracture, in *Hydraulic Fracturing Stress Measurements*, edited by M. D. Zoback and B. C. Haimson, pp. 159-166, National Academy Press, Washington, D. C., 1983.
- Richardson, R. M., Hydraulic fracture in arbitrarily oriented boreholes: An analytic approach, in *Hydraulic Fracturing Stress Measurements*, edited by M. D. Zoback and B. C. Haimson, pp. 167-175, National Academy Press, Washington, D. C., 1983.
- Rogers, A. M., S. C. Harmsen, W. J. Carr, and W. Spence, Southern Great Basin seismicological data report for 1981 and preliminary data analysis, *U.S. Geol. Surv. Open File Rep.*, 83-669, 1983.
- Scott, R. B., and J. Bonk, Preliminary geologic map of Yucca Mountain with geologic sections, Nye County, Nevada, *U.S. Geol. Surv. Open File Rep.*, 84-494, 1984.
- Scott, R. B., and M. Castellanos, Stratigraphic and structural relations of volcanic rocks in drill holes USW GU-3 and USW G-3, Yucca Mountain, Nye County, Nevada, *U.S. Geol. Surv. Open File Rep.*, 84-0491, 1984.
- Smith, C., W. C. Vollendorf, and W. E. Warren, In-situ stress from hydraulic fracture measurements in G Tunnel, Nevada Test Site, *Rep. SAND80-1138*, Sandia Natl. Lab., Albuquerque, N. M., 1981.
- Smith, R. B., and A. G. Lindh, Fault-plane solutions of the western United States: A compilation, Cenozoic Tectonics and Regional Geophysics of the Western Cordillera, *Mem. Geol. Soc. Am.*, 152, 107-109, 1978.
- Snyder, R. P., Composite potshot fracture map of Pahute Mesa, Nevada Test Site, Special Studies-86, *U.S. Geol. Surv. Rep. USGS-474-100*, 1971.
- Snyder, D. B., and W. J. Carr, Interpretation of gravity data in a complex volcano-tectonic setting, southwestern Nevada, *J. Geophys. Res.*, 89, 10193-10206, 1984.
- Spengler, R. W., F. M. Byers, and J. B. Warner, Stratigraphy and structure of volcanic rocks in drill hole USW-G1, Yucca Mountain, Nye County, Nevada, *U.S. Geol. Surv. Open File Rep.*, 81-1349, 1981.
- Springer, J. E., and R. K. Thorpe, Borehole elongation versus in situ stress orientation, *Rep. UCRL-87018*, Lawrence Livermore Lab., Livermore, Calif., 1981.
- Stock, J. M., and J. H. Healy, Magnitudes and orientations of stresses in an extensional regime: Yucca Mountain, Nevada, *Geol. Soc. Am. Abstr. Programs*, 16, 669, 1984.
- Stock, J. M., J. H. Healy, and S. H. Hickman, Report on televiewer log and stress measurements in core hole USW G-2, Nevada Test Site, *U.S. Geol. Surv. Open File Rep.*, 84-172, 1984.
- Swadley, W. C., D. L. Hoover, and J. N. Roebolt, Preliminary report on Late Cenozoic faulting and stratigraphy in the vicinity of Yucca Mountain, Nye County, Nevada, *U.S. Geol. Surv. Open File Rep.*, 84-788, 1984.
- Vaniman, D., and B. Crowe, Geology and petrology of the basalts of Crater Flat: Applications to volcanic risk assessment for the Nevada Nuclear Waste Storage Investigations, *Rep. LA-8345-MS*, Los Alamos Natl. Lab., Los Alamos, N. M., 1981.
- Winograd, I. J., Radioactive waste disposal in thick unsaturated zones, *Science*, 212(4302), 1457-1464, 1981.
- Zemanek, J., R. L. Caldwell, E. E. Glenn, S. V. Holcomb, L. J. Norton, and A. J. D. Straus, The borehole televiewer—A new logging concept for fracture location and other types of borehole inspection, *J. Pet. Technol.*, 21, 702-774, 1969.
- Zemanek, J., E. E. Glenn, L. J. Norton, and R. L. Caldwell, Formation evaluation by inspection with the borehole televiewer, *Geophysics*, 35, 254-269, 1970.
- Zoback, M. D., and J. H. Healy, Friction, faulting, and in situ stress, *Ann. Geophys.*, 2, 689-698, 1984.
- Zoback, M. D., and S. Hickman, In situ study of the physical mechanisms controlling induced seismicity at Monticello Reservoir, South Carolina, *J. Geophys. Res.*, 87, 6959-6974, 1982.
- Zoback, M. D., D. Moos, L. Martin, and R. N. Anderson, Well bore breakouts and in situ stress, *J. Geophys. Res.*, 90, 5523-5530, 1985.
- Zoback, M. L., and M. D. Zoback, State of stress in the conterminous United States, *J. Geophys. Res.*, 85, 6113-6156, 1980.

J. H. Healy, Office of Earthquakes, Volcanoes, and Engineering, U.S. Geological Survey, Menlo Park, CA 94025.
 S. H. Hickman and J. M. Stock, Department of Earth, Atmospheric, and Planetary Sciences, MIT, Cambridge, MA 02139.
 M. D. Zoback, Department of Geophysics, Stanford University, Stanford, CA 94305.

(Received August 17, 1984;
 revised May 22, 1985;
 accepted May 24, 1985.)